The Impact of Monthly Variation of the Pacific-North America (PNA) Teleconnection Pattern on Wintertime Surface-layer Aerosol Concentrations in the United States

Jin Feng[1,2], Hong Liao[1,*], Jianping Li[3]

[1]State key Laboratory of Atmospheric Boundary Layer Physics and Atmospheric Chemistry, Institute of Atmospheric Physics, Chinese Academy of Sciences, Beijing, China

[2]University of Chinese Academy of Science, Beijing, China

[3]College of Global Change and Earth System Science of Beijing Normal University, Beijing, China

*Corresponding author address:

Prof. Hong Liao

LAPC, Institute of Atmospheric Physics

Chinese Academy of Sciences

Beijing 100029, China

E-mail: hongliao@mail.iap.ac.cn

Abstract

The Pacific-North America teleconnection (PNA) is the leading general circulation pattern in the troposphere over the region of North Pacific to North America during wintertime. This study examined the impacts of monthly variation of the PNA phase (positive or negative phase) on wintertime surface-layer aerosol concentrations in the U.S. by analyzing observations during 1999–2013 from the Air Quality System of the Environmental Protection Agency (EPA-AQS) and the model results for 1986–2006 from the global three-dimensional Goddard Earth Observing System (GEOS) chemical transport model (GEOS-Chem). The composite analyses on the EPA-AQS observations over 1999–2013 showed that the average concentrations of $PM_{2.5}$, sulfate, nitrate, ammonium, organic carbon, and black carbon aerosols over the U.S. were higher in the PNA positive phases than in the PNA negative phases by 1.0 μg m^{-3} (8.7%), 0.01 μg m^{-3} (0.5%), 0.3 μg m^{-3} (29.1%), 0.1 μg m^{-3} (11.9%), 0.6 μg m^{-3} (13.5%), and 0.2 μg m^{-3} (27.8%), respectively. The simulated geographical patterns of the differences in concentrations of all aerosol species between the PNA positive and negative phases were similar to observations. Based on the GEOS-Chem simulation driven by the assimilated meteorological fields, the PNA-induced variation in planetary boundary layer height was found to be the most dominant meteorological factor that influenced the concentrations of $PM_{2.5}$, sulfate, ammonium, organic carbon, and black carbon, and the PNA-induced variation in temperature was the most important parameter that influenced nitrate aerosol. Results from this work have important implications for understanding and prediction of air quality in the United States.

1 Introduction

Aerosols are the major air pollutants that have adverse effects on human health, reduce atmospheric visibility, and influence climate through aerosol-radiation and aerosol-cloud interactions (IPCC, 2013). Aerosol concentrations are high over the industrialized regions such as the U.S., Europe, and East Asia, which are driven by emissions of aerosols and aerosol precursors (Dutkiewicz et al. 2000; Vestreng et al. 2007; Hand et al. 2012a; Mijling et al. 2013) and regional meteorological conditions.

Previous studies have shown that aerosol concentrations are very sensitive to meteorological parameters (Aw and Kleeman 2003; Wise and Comrie 2005; Dawson et al. 2007; Kleeman 2008; Jacob and Winner 2009; Tai et al. 2010; Tai et al. 2012a; Allen et al. 2015; Markakis et al. 2015; Megaritis et al. 2014; Porter et al. 2015). Aw and Kleeman (2003) examined the sensitivity of $PM_{2.5}$ (aerosol particles which diameter ≤ 2.5 μm) concentration to temperature by performing sensitivity studies in the California Institute of Technology/UC Davis (CIT/UCD) air quality model. A cross-board increase in temperature by 5 K in Southern California on September 25, 1996, led to decreases in peak $PM_{2.5}$ concentrations by up to 30.7 μg m^{-3} (~30%). Wise and Comrie (2005) reported, by statistical analyses of observational datasets obtained from Air Quality System of U.S. Environmental Protection Agency (EPA-AQS), that the variations in meteorological parameters accounted for 20–50% of the variability in aerosol levels over 1990–2003 in five metropolitan areas in the southwestern U.S.. They found that aerosols in these five cities were most sensitive to relative humidity. Dawson et al. (2007) found, by sensitivity studies in the Particulate Matter Comprehensive Air Quality Model with extensions (PMCAMx), that $PM_{2.5}$ concentrations in summer had a small sensitivity to temperature increases (−16 ng m^{-3} K^{-1} on average) because the increases in sulfate offset the decreases in

74 nitrate and organics, while $PM_{2.5}$ concentrations in winter decreased significantly with
75 temperature (−170 ng m^{-3} K^{-1} on average) because the increases in temperature led
76 to large reductions in nitrate and organics. Dawson et al. (2007) also showed that
77 $PM_{2.5}$ concentrations increased with humidity in both winter and summer. Jacob and
78 Winner (2009) summarized by literature review that the regional stagnation, mixing
79 depth, and precipitation are the most important meteorological parameters that
80 influence surface-layer aerosol concentrations. Future climate change was also
81 simulated to influence aerosol levels over the U.S. by about 1 μg m^{-3} (Jacob and
82 Winner 2009), as a result of the climate-induced changes in atmospheric oxidants,
83 transport, deposition, and the shift of gas-particle equilibria (Liao et al. 2006; Unger et
84 al. 2006; Bauer et al. 2007; Jacob and Winner 2009; Pye et al. 2009; Lam et al. 2011;
85 Day and Pandis 2011; Juda-Rezler et al. 2012; Tai et al. 2012b).

86 Previous studies have also reported that the changes in atmospheric circulation
87 pattern and climate systems, such as the East Asian Summer Monsoon (EASM),
88 North Atlantic Oscillation (NAO), El Nino-South Oscillation (ENSO), Atlantic
89 Multidecadal Oscillation (AMO), and Arctic sea ice (ASI), can modulate distributions
90 and concentrations of aerosols (Moulin et al. 1997; Singh and Palazoglu 2012; Zhu et
91 al. 2012; Jerez et al. 2013; Liu et al. 2013; Xiao et al. 2014; Wang et al. 2015). Zhu et
92 al. (2012) found, by simulation of aerosol concentrations over years 1986–2006 with
93 the global chemical transport model GEOS-Chem, that the decadal-scale weakening
94 of the EASM led to increases in aerosol concentrations in eastern China, and
95 summertime surface aerosol concentrations in the weakest EASM years were larger
96 than those in the strongest EASM years by approximately 20%. Moulin et al. (1997)
97 showed that the variations in NAO could influence mineral dust aerosol transported to
98 the North Atlantic Ocean and the Mediterranean Sea, since the mean aerosol optical

depth (AOD) of dust in summer correlated with the NAO index during 1983–1994 with a correlation coefficient of 0.50. Jerez et al. (2013) found, by simulations of aerosols for years 1970–1999 with the CHIMERE chemistry transport model driven by the BCMWF ERA40 reanalysis data, that the concentrations of PM_{10} and $PM_{2.5}$ in the southern European regions in winter differed by 10 and 20 μg m^{-3}, respectively, between the positive and negative NAO phases. By using the multi-angle imaging spectroradiometer satellite (MISR) datasets of AOD during 2000–2011, Liu et al. (2013) found a period of 3–4 years in observed summertime AOD over the North China Plain (NCP), and the peak of summertime AOD in NCP occurred four months later after the rapidly transition of El Nino from a warm phase to a cold phase because of the associated cyclone anomaly and maritime inflow over the NCP. Singh and Palazoglu (2012) found correlations between PDO and ENSO and the aerosol exceedance days (defined as the days with $PM_{2.5}$ concentrations larger than the U.S. National Ambient Air Quality Standard) at 6 regions in the U.S. by using the EPA-AQS $PM_{2.5}$ wintertime datasets during 1950–2008.

The Pacific-North America teleconnection pattern (PNA) is one of the most recognized, influential climate patterns in the mid-latitudes over the region of North Pacific to North America during wintertime with monthly variations (Wallace and Gutzler 1981; Blackmon et al. 1984; Liang et al. 2005; Athanasiadis and Ambaum 2009). The PNA phase is defined by the geopotential height anomalies in the middle troposphere over the vicinity of Hawaii, the south of the Aleutian Islands, the intermountain region of North America, and the Gulf Coast region in the U.S. (Wallace and Gutzler 1981). A positive (negative) PNA phase is characterized by positive (negative) geopotential height anomalies over the vicinity of Hawaii and the northwestern North America, while negative (positive) geopotential height anomalies

over south of the Aleutian Islands and the Gulf Coast region (see Fig. S1 in the auxiliary material).

The PNA has large impacts on surface-layer meteorological variables in the U.S. during wintertime. Previous studies have reported strong positive (negative) correlation between PNA and surface ambient temperature in the northwestern (southeastern) U.S. (Leathers et al. 1991; Redmond and Koch 1991; Liu et al. 2015), and negative correlation between PNA and precipitation rate (Leathers et al. 1991; Coleman and Rogers 2003; Ning and Bradley 2014; 2015) and moisture (Coleman and Rogers 2003) in the contiguous Ohio River Valley. These variations in meteorological parameters in the U.S. are associated with the PNA-induced anomalies in jet stream position, activities of cold fronts, and synoptic cyclones (Leathers et al. 1991; Notaro et al. 2006; Myoung and Deng 2009).

Several studies have examined the impacts of PNA on aerosols. Gong et al. (2006) studied the interannual variations in the trans-Pacific transport of Asian dust during 1960–2003 by using the Northern Aerosol Regional Climate Model (NARCM). They found a negative correlation (with a correlation coefficient of –0.55) between the PNA and the ratio of dust mass that reached the North American continent to that exported from Asia because of the strong westerly jet in the East Pacific during the negative PNA phases. Di Pierro et al. (2011), by using satellite retrieval of aerosol optical depth (AOD) from Cloud-Aerosol Lidar with Orthogonal Polarization (CALIOP), identified 11 events of Asian aerosol transport to the Arctic during 2007 to 2009, in which 4 events were associated with the negative PNA phases. These studies, however, were focused on the impact of PNA on the transport of aerosols due to the variations in westerly jet stream and blocking activity. Furthermore, these studies were limited to aerosols in the regions of North America and the Arctic.

We examine in this work the impacts of monthly variations in PNA phase on aerosol concentrations in the U.S. during wintertime, by analyses of the observed aerosol concentrations during 1999–2013 from EPA-AQS and also by simulations of aerosol concentrations for years 1986–2006 using the global chemical transport model GEOS-Chem. The scientific goals of this work are (1) to quantify the differences in wintertime concentrations of sulfate (SO_4^{2-}), nitrate (NO_3^-), ammonium (NH_4^+), black carbon (BC), organic carbon (OC), and $PM_{2.5}$ in the U.S. between different PNA phases, and (2) to understand the roles of PNA-induced variations in meteorology (for example, surface air temperature, wind speed, planetary boundary layer height, precipitation, and relative humidity) in influencing the wintertime aerosol concentrations. The definition of the PNA index, the EPA-AQS observation data used in this work, and the numerical simulation with the GEOS-Chem model are described in Sect. 2. Sections 3 and 4 present the impacts of the PNA on wintertime aerosol concentrations in the U.S. obtained from the EPA-AQS observations and the GEOS-Chem simulation, respectively. The mechanisms for the impacts of PNA on aerosols are examined in Sect. 5.

2 Data, simulation, and methodology

2.1 Observed aerosol concentrations

Observed concentrations of aerosols are obtained from the Air Quality System of the U.S. Environmental Protection Agency (EPA-AQS, http://www.epa.gov/airquality/airdata/). The EPA-AQS daily $PM_{2.5}$ mass concentrations are available over 1999–2013 at about 1200 sites, and the speciated aerosol concentrations, including those of SO_4^{2-}, NO_3^-, NH_4^+, BC and OC, are available for 2000–2013 at about 300 sites.

The measurements of aerosol concentrations from the EPA-AQS were carried out at various time intervals (for example, with measurements every one, three or six days) at different sites, and there were plenty of missing values at many sites. The observed concentrations are pre-processed following the three steps: (1) For a specific site, the observations are used in our analyses if the site had at least 5 months of observations and there were at least 5 observation records within each month. (2) The mean seasonal cycle in aerosol concentrations in the months of November-March is removed by using the similar approach to that used for PNA index (see Sect. 2.3 below). Such deseasonality approach was used in previous studies that examined the monthly variations in mineral dust aerosol (Cakmur et al. 2001; Mahowald et al. 2003), the decreasing trends in observed $PM_{2.5}$ concentrations and satellite AOD in the southeastern U.S. over 2000–2009 (Alston et al. 2012), and the monthly variations in global AOD (Li et al. 2013). (3) Since the observed aerosol concentrations exhibited a significant decreasing trend from 1999 to present in the U.S. due to the reductions in emissions of aerosols and aerosol precursors (Alston et al. 2012, http://www3.epa.gov/airtrends/aqtrends.html#comparison), the long-term linear trend in concentrations is identified by the least-square fit and then removed from the observed concentrations for each site. The EPA-AQS sites with measurements that meet the criteria described in (1) are shown in Fig. 1.

2.2 GEOS-Chem Simulation

We also examine the impacts of PNA on simulated aerosol concentrations in the U.S. by using the GEOS-Chem model (version 8-2-1, http://acmg.seas.harvard.edu/geos). The GEOS-Chem model is a global chemical transport model driven by the assimilated meteorological fields from the Goddard Earth Observing System (GEOS) of the NASA Global Modeling and Assimilation Office (GMAO). The version of the

model we use has a horizontal resolution of 2° ×2.5° and 30 hybrid sigma-P layers from the surface to 0.01 hPa altitude. The model has a fully coupled simulation of tropospheric O_3-NO_x-VOC chemistry and aerosols including SO_4^{2-}, NO_3^-, NH_4^+, BC, OC (Park et al. 2003; Park et al. 2004), mineral dust (Fairlie et al. 2007), and sea salt (Alexander et al. 2005). Considering the large uncertainties in chemistry schemes of secondary organic aerosol (SOA), SOA in our simulation is assumed to be the 10% carbon yield of OC from biogenic terpenes (Park et al., 2003) and 2% carbon yield of OC from biogenic isoprene (van Donkelaar et al., 2007; Mu and Liao, 2014). We mainly examine simulated anthropogenic aerosols from the GEOS-Chem simulation, since mineral dust concentrations in winter are very small (Malm et al. 2004; Zhang et al. 2013) and sea salt is not a major aerosol species in the U.S. (Malm et al. 2004).

The model uses the advection scheme of Lin and Rood (1996), the deep convective scheme of Zhang and McFarlane (1995), the shallow convection scheme of Hack (1994), the wet deposition scheme of Liu et al. (2001), and the dry deposition scheme of Wesely (1989) and Wang et al. (1998). The instantaneous vertical mixing in the planetary boundary layer (PBL) is accounted for by the TURBDAY mixing scheme (Bey et al., 2001). The PBL occupies the lowest 3–6 vertical model layers over the U.S..

We simulate aerosols for years of 1986–2006 driven by the GEOS-4 reanalysis data. The years of 1986–2006 are chosen for chemistry-aerosol simulation because these are the years that the GEOS-4 datasets are available. Global anthropogenic emissions are from the Global Emissions Inventory Activity (GEIA) (Park et al. 2004; Park et al. 2006; Zhu et al. 2012; Yang et al. 2015). Anthropogenic emissions over the U.S. are overwritten by the U.S. EPA National Emission Inventory for 1999 (NEI99), which have monthly variations in emissions of precursors including SO_2, NO_x, and

224 NH_3. Monthly biomass burning emissions are taken from the Global Fire Emissions
225 Database version 2 (GFED-2) (Giglio et al. 2006; van der Werf et al. 2006). During
226 the simulation of aerosols for years of 1986–2006, the global anthropogenic and
227 biomass burning emissions of aerosols and aerosol precursors are fixed at year 2005
228 levels, so that the variations in aerosol concentrations are caused by variations in
229 meteorological parameters (PNA phases) alone.

230 Natural emissions of O_3 precursors, including biogenic NMVOCs and NO_x from
231 lighting and soil, are allowed to vary over 1986–2006 following the variations in the
232 GEOS-4 meteorological parameters. Biogenic NMVOC emissions are calculated
233 using the module of Model of Emissions of Gases and Aerosols from Nature
234 (Guenther et al. 2006). Lightning NO_x emissions are described by Sauvage et al.
235 (2007) and Murray et al. (2012). Soil NO_x emissions are calculated using the
236 algorithm proposed by Yienger and Levy (1995).

237 The GEOS-Chem simulation of aerosols in the U.S. have been evaluated
238 extensively by previous studies (Park et al. 2003; Park et al. 2004; Park et al. 2005;
239 Heald et al. 2006; van Donkelaar et al. 2006; Liao et al. 2007; Heald et al. 2008; van
240 Donkelaar et al. 2008; Fu et al. 2009; Drury et al. 2010; Leibensperger et al. 2011;
241 Zhang et al. 2012). These studies have shown that the GEOS-Chem model can
242 capture the magnitudes and distributions of aerosols in the U.S..

243 **2.3 PNA index**

244 The PNA index (PNAI) is commonly used to quantify the changes in PNA phase
245 (Wallace and Gutzler 1981; Leathers et al. 1991). This study follows the definition of
246 PNAI by Leathers et al. (1991). In order to examine the monthly variations in PNA, the
247 mean seasonal cycle of geopotential height at 700 hPa is removed for the months of
248 November, December, January, February, and March (NDJFM) in the studied years.

Such deseasonality approach has been used in the analyses of the growth and decay of PNA phase in NDJFM (Feldstein 2002), the development of NAO (Feldstein 2003), the influence of NAO on precipitation in Europe (Qian et al. 2000), and the variations in Madden–Julian oscillation (Wheeler and Hendon 2004). If we are concerned with the PNAI during *n* years, the monthly PNAI in month *j* (*j* is one of the 5 months of NDJFM) of year *i* is calculated by:

$$PNAI = \frac{1}{3}\left[-Z^{*\prime}_{i,j}(47.9°N, 170°W) + Z^{*\prime}_{i,j}(47.9°N, 110°W) - Z^{*\prime}_{i,j}(29.7°N, 86.3°W)\right] \quad (1)$$

where $Z^{*\prime}_{i,j} = \frac{Z'_{i,j}}{\sqrt{\frac{1}{n\times 5}\sum_{i=1}^{n}\sum_{j=1}^{5} {Z'_{i,j}}^2}}$ and $Z'_{i,j} = Z_{i,j} - \frac{1}{n}\sum_{i=1}^{n} Z_{i,j}$. Therefore, $Z'_{i,j}$ denotes the removal of seasonal cycle, and $Z^{*\prime}_{i,j}$ denotes the standardized anomaly of geopotential height at 700 hPa in month *j* of year *i* with seasonal-cycle removed.

The PNAI is calculated by using both the National Center of Environmental Prediction-Department of Energy Atmospheric Model Inter-comparison Project Reanalysis data (NCEP-2, horizontal resolution 2.5°×2.5° globally, http://www.esrl.noaa.gov/psd/data/gridded/data.ncep.reanalysis2.html) for years of 1986–2013 (referred to as NCEP2-PNAI) and the GEOS-4 assimilated meteorological data (referred to as GEOS4-PNAI) for 1986–2006 (Fig. 2). Both series of PNA index show strong monthly variations (Fig. 2), and the GEOS4-PNAI agrees with NCEP2-PNAI over 1986–2006 with a high correlation coefficient of 0.99, indicating that the NCEP-2 and GEOS-4 datasets are consistent in representing the monthly variations of PNAI.

There are n×5 PNAI values for *n* years, since we calculate PNAI for the months of NDJFM of each year. These *n*×5 PNAI values are classified into 3 categories for our composite analyses of aerosol concentrations and meteorological parameters: the positive PNA months (PNA+) that are 25% of the *n*×5 PNAI months with the highest

273 positive PNAI values, the negative PNA months (PNA–) that are 25% of the $n\times5$ PNAI
274 months with the highest negative PNAI values, and the rest months that are referred
275 to as the transitional months (Fig. 2).
276
277 **3 Impacts of PNA on observed aerosol concentrations**
278 The measurements of $PM_{2.5}$ are available over 1999–2013, in which there were 18
279 PNA+ months and 18 PNA– months as shown in Fig. 2a. Figure 3 shows the
280 differences in observed surface-layer $PM_{2.5}$ concentrations between the PNA+ and
281 PNA– months (concentrations averaged over the 18 PNA+ months minus those
282 averaged over the 18 PNA– months). The uncertainty associated with the differences
283 in aerosol concentrations between PNA+ and PNA– months is represented by the
284 two-tail Student-t test with significance level of 90%. Among 1044 sites with $PM_{2.5}$
285 concentrations (Fig.1), 42% of which had statistically significant differences in $PM_{2.5}$
286 between PNA+ and PNA– months. Relative to the PNA– months, $PM_{2.5}$
287 concentrations in PNA+ months were higher in California, the contiguous Salt Lake
288 (northern Utah), and over and near the eastern Midwest. The enhancement of $PM_{2.5}$
289 reached 7–9 μg m^{-3} (or 40–80%) in California, 7–9 μg m^{-3} (80–100%) around the Salt
290 Lake, 3–5 μg m^{-3} (40–80%) over and near the eastern Midwest. At sites in North
291 Dakota, Wisconsin, Michigan, Minnesota, Montana, Texas and Maine, the $PM_{2.5}$
292 concentrations were lower by up to 2 μg m^{-3} (–10 to –20%) in PNA+ months than in
293 PNA– months. As the concentrations are averaged over all sites (including the sites
294 that pass and do not pass the t-test with 90% confidence level) in the U.S., the
295 western U.S. (west of 100°W, Fig.1), and the eastern U.S. (east of 100°W, Fig. 1),
296 $PM_{2.5}$ concentrations were higher by 1.0 μg m^{-3} (8.7%), 1.3 μg m^{-3} (14.3%), and 0.8
297 μg m^{-3} (7.2%), respectively, in the PNA+ months than in PNA– months (Table 1).

298 The measurements of speciated aerosols are available during 2000–2013, in
299 which there were 17 PNA+ and 17 PNA– months (Fig. 2b). Figure 3 also shows the
300 differences in observed surface-layer concentrations of individual aerosol species
301 between the PNA+ and PNA– months. The differences in concentrations of SO_4^{2-},
302 NO_3^- and NH_4^+ show statistically significant positive values at most sites. Among the
303 355, 343, and 194 sites with measurements of SO_4^{2-}, NO_3^- and NH_4^+, 30%, 44%, and
304 39% of which pass the two-tail t-test with 90% confidence level, respectively. While
305 the absolute differences in concentrations of SO_4^{2-}, NO_3^- and NH_4^+ between PNA+
306 and PNA– were in the range of 0–1 μg m^{-3} at most sites, the maximum differences
307 reached 1.5–2.5 μg m^{-3} (30–50%) for SO_4^{2-} in Pennsylvania, 1.5–2.5 μg m^{-3} (150–
308 200%) for NO_3^- in Illinois, Indiana and Ohio, and 1.5–2.5 μg m^{-3} (50–70%) for NH_4^+ in
309 Pennsylvania. Averaged over the sites with measurements, the absolute differences
310 in concentrations of SO_4^{2-} and NO_3^- between PNA+ and PNA– months were larger in
311 the eastern U.S. than in the western U.S.. As shown in Table 1, the differences in the
312 averaged concentrations of SO_4^{2-}, NO_3^- and NH_4^+ were, respectively, 0.1 μg m^{-3}
313 (3.7%), 0.4 μg m^{-3} (36.5%), and 0.1 μg m^{-3} (10.5%) in the eastern U.S., 0.03 μg m^{-3}
314 (3.2%), 0.2 μg m^{-3} (23.8%), and 0.2 μg m^{-3} (31.6%) in the western U.S., as well as
315 0.01 μg m^{-3} (0.5%), 0.3 μg m^{-3} (29.1%), and 0.1 μg m^{-3} (11.9%) in the whole of U.S..
316 With regard to carbonaceous aerosols, among the 105 and 104 sites with
317 measurements of OC and BC, 39% and 31% of which pass the two-tail t-test with 90%
318 confidence, respectively. The differences in concentrations of these two species
319 between PNA+ and PNA– months show similar geographical pattern, with positive
320 values at most sites but negative values in Michigan, New York, and the South
321 Atlantic States. The maximum differences between the PNA+ and PNA– months
322 reached 2.5–3 μg m^{-3} (50–70%) in Kentucky for OC. Averaged over sites with

measurements available, the absolute differences in OC and BC concentrations between the PNA+ and PNA– months were larger in the western U.S. than in the eastern U.S. (Table 1). Among all aerosol species listed in Table 1, OC exhibited the largest absolute differences between the PNA phases in the western U.S., because OC accounts for 25–65% of $PM_{2.5}$ in the western U.S. (Malm et al. 2004) and the OC observed by EPA-AQS network, which are located in urban and suburban settings, were higher than the observations by other long term networks in U.S..(Malm et al. 2011, Rattigan et al. 2011, Hand et al. 2012b, 2014).

Observations from EPA-AQS datasets indicate the large impacts of PNA phase on aerosol concentrations in the U.S.. It should be noted that, in our analyses above, the locations of measurements and the numbers of samples were different for different aerosol species. The regional averages were also influenced by the uneven distributions of observational sites in different regions. Therefore, model results from the GEOS-Chem simulation will be used to further analyze the impacts of PNA on aerosols in the U.S., as presented in the subsequent sections.

We have also calculated the correlation coefficient between PNAI and EPA-AQS surface aerosol concentrations at each site for each aerosol species ($PM_{2.5}$, SO_4^{2-}, NO_3^-, NH_4^+, OC, or BC) (see auxiliary Fig. S2). At most sites, positive (negative) correlation coefficients in Fig. S2 corresponded to the increases (decreases) in aerosol concentration in PNA+ months relative to PNA– months shown in Fig. 3. Positive correlation coefficients were large over California, the contiguous Salt Lake, and over and near the eastern Midwest. The fraction of temporal variability explained by PNA (FTVEP) can be quantified approximately by the square of correlation coefficient (http://mathbits.com/MathBits/TISection/Statistics2/correlation.htm) (see auxiliary Fig. S3). For all aerosol species, FTVEP were about 5–15% at most sites.

For $PM_{2.5}$, SO_4^{2-}, NO_3^- and NH_4^+ aerosols, FTVEP values were high over and near the eastern Midwest, where the PNA teleconnection explained up to 50%, 40%, 50%, and 40% of temporal variances of surface concentrations of these aerosol species, respectively.

4 Impacts of PNA on simulated aerosol concentrations

4.1 Simulated aerosol concentrations and model evaluation

Fig. 4a shows the simulated surface-layer concentrations of $PM_{2.5}$ (the sum of SO_4^{2-}, NO_3^-, NH_4^+, BC, and OC) and each aerosol species averaged over NDJFM of 1999–2006. These years are selected because they are the common years of model results and EPA-AQS observation datasets. The simulated $PM_{2.5}$ concentrations were higher in the eastern U.S. than in the western U.S.. The maximum surface $PM_{2.5}$ concentrations reached 14–16 μg m^{-3} in Ohio and Pennsylvania. $PM_{2.5}$ concentrations in the western U.S. were generally less than 4 μg m^{-3}, except for California where $PM_{2.5}$ concentrations were 2–6 μg m^{-3}. The distribution of SO_4^{2-} was similar to that of $PM_{2.5}$, with higher concentrations in the eastern U.S. (1–8 μg m^{-3}) than in the western U.S. (0–3 μg m^{-3}) due to the coal-fired power plants in the Midwest (Park et al. 2006). The concentrations of NO_3^- and NH_4^+ were the highest over and near the eastern Midwest, with values of 3–4 and 2–3 μg m^{-3}, respectively. The maximum OC concentrations were simulated to be 2–3 μg m^{-3} in two regions, from Ohio to Massachusetts and from Alabama to South Carolina. The simulated BC concentrations in the U.S. were 0–1 μg m^{-3}, except for the contiguous New York where BC concentrations reached 1–2 μg m^{-3}. The magnitudes and geographic distributions of SO_4^{2-}, NO_3^-, NH_4^+ concentrations simulated in our work are similar to

372 those simulated by Park et al. (2006) and Pye et al. (2009), and our simulated OC
373 and BC were similar to those reported by Park et al. (2003).

374 Figure 4b presents the scatter plots of the simulated concentrations versus the
375 EPA-AQS observations. The simulated $PM_{2.5}$ concentrations had normalized mean
376 bias ($NMB = \sum_{m=1}^{M}(S_m - O_m) / \sum_{m=1}^{M}(O_m) \times 100\%$, where S_m and O_m are the
377 simulated and observed aerosol concentrations in month *m*, respectively. *M* is the
378 total number of winter months examined) of –30% over the U.S., and the correlation
379 coefficient between simulated and observed $PM_{2.5}$ concentrations was 0.57. The
380 simulated wintertime SO_4^{2-}, NO_3^- and NH_4^+ had NMBs of 37%, 4%, and 26%,
381 respectively. Similar bias in simulated SO_4^{2-} in December-January-February (DJF)
382 was reported Park et al. (2006), as the GEOS-Chem model results were compared
383 with observations from the Clean Air Status and Trends Network (CASTNET). The
384 high bias in our simulated NH_4^+ was associated with the overestimation of SO_4^{2-}. Our
385 model underestimates $PM_{2.5}$, SO_4^{2-}, NO_3^-, NH_4^+, OC and BC in the western U.S. (Fig.
386 4b), which can be explained in part by the relatively high aerosol concentrations
387 observed for this region from the EPA-AQS. Hand et al. (2014) compared the
388 observed concentrations of aerosols from the EPA-AQS with those from the
389 Interagency Monitoring of Protected Visual Environments (IMPROVE) for 2008–2011,
390 and showed that the ratios of wintertime aerosol concentrations of ammonium sulfate,
391 ammonium nitrate, OC, and BC from the EPA-AQS to those from the IMPROVE were,
392 respectively, 2.3, 7.7, 8.3, and 13.1, as the concentrations were averaged over the
393 western U.S.. Liu et al. (2004) also attributed the high EPA-AQS concentrations in the
394 western U.S. to the relative sparse urban sites that were heavily influenced by strong
395 local sources such as automobiles and wood fires. The low model biases in the
396 western U.S. may also be caused by the biases in emissions in the model.

Since this study is dedicated to examine the influence of PNA phase on the month-to-month variations of aerosol concentrations during wintertime, Fig. 4c compares, for each aerosol species, the deviation from the mean (DM) of observed concentration with that of simulated concentration for each winter month. The DM is defined as $DM_m = \left(C_m - \frac{1}{M}\sum_{m=1}^{M} C_m\right) / \frac{1}{M}\sum_{m=1}^{M} C_m$, where C_m is the simulated average aerosol concentration over the U.S. in month *m*, and *M* is the number of winter months examined (we consider the months of NDJFM over 1999–2006 for $PM_{2.5}$, and the months of NDJFM over 2000–2006 for SO_4^{2-}, NO_3^-, NH_4^+, BC, and OC). The model captures fairly well the peaks and troughs of DMs for $PM_{2.5}$, SO_4^{2-}, NO_3^- and NH_4^+, with correlation coefficients of 0.61, 0.45, 0.33, and 0.65, respectively. The model does not capture well the monthly variations of DMs of concentrations of OC and BC, because both anthropogenic and biomass burning emissions are fixed at year 2005 levels during our simulation over 1986–2006 to isolate the impacts of variations in meteorological parameters (PNA phases) on aerosols (see Sect. 2.2). Since the biomass burning emissions, which contribute largely to carbonaceous aerosols, have large interannual variations (Duncan et al., 2003; Generoso et al., 2003; van der Werf et al., 2006), we also show in Fig. 4c the time series of DMs of biomass burning emissions of OC and BC by using biomass burning emissions in NDJFM over 2000–2006 from GFED v2. The correlation coefficients between biomass burning emissions and observed concentrations of OC and BC were 0.36 and 0.34, respectively, indicating that the observed variations in OC and BC were influenced by monthly and interannual variations in biomass burning. We have also calculated the temporal correlation coefficient between EPA-AQS observations and GEOS-Chem model results at each site for each aerosol species (auxiliary Fig. S4). The temporal correlations were statistically significant for $PM_{2.5}$, SO_4^{2-}, NO_3^-, NH_4^+ at

most sites in the U.S., especially over and near the eastern Midwest where largest increases in aerosol concentrations were identified in the PNA+ months relative to the PNA– months.

4.2 Impact of PNA on simulated surface-layer aerosol concentrations

We have performed the GEOS-Chem simulation for years 1986–2006, in which there were 35 PNA+ and 35 PNA– months (Fig. 2). Figure 5a shows the concentrations of $PM_{2.5}$ and each aerosols species (SO_4^{2-}, NO_3^-, NH_4^+, BC, and OC) averaged over the PNA– months of 1986–2006. The magnitudes and geographic distributions of aerosol concentrations in PNA– months were similar to those averaged over NDJFM of years 1999–2006 in Fig. 4.

The simulated absolute and relative differences in aerosol concentrations between PNA+ and PNA– months are shown in Figs. 5b and 5c. The $PM_{2.5}$ concentrations over the U.S. are simulated to increase in PNA+ relative to PNA– months. The maximum enhancement in $PM_{2.5}$ concentrations in PNA+ months was 1.8–2.4 μg m^{-3} (20–40%), located in the juncture of Tennessee and Arkansas. Note that the pattern of simulated differences in $PM_{2.5}$ between PNA+ and PNA–months was similar to that of observations (Fig. 3), except that the simulated differences were not large in California, mainly due to the underestimation of OC in California as compared to EPA-AQS data (Fig. 4b). The simulated $PM_{2.5}$ concentrations were higher by 0.6 μg m^{-3} (12.2%), 0.3 μg m^{-3} (14.0%), and 0.9 μg m^{-3} (10.8%) over the whole of, western, and eastern U.S., respectively, in the PNA+ months than in PNA– months (Table 2). The simulated relative difference in $PM_{2.5}$ was close to that from observations (Table 1) in the western U.S., but the simulated relative differences in $PM_{2.5}$ were larger than those from observations in the eastern and whole of U.S..

447 Fig. 5 also shows the differences in simulated surface-layer concentrations of
448 SO_4^{2-}, NO_3^- and NH_4^+ between the PNA+ and the PNA– months. The differences in
449 concentrations of SO_4^{2-} were larger in the western than in the eastern U.S., with
450 maximum enhancements of 0.4–0.8 μg m^{-3} (30–50%) over the West North Central
451 States (South Dakota, Nebraska, Minnesota, Iowa, and Missouri). The differences in
452 concentrations of NO_3^- and NH_4^+ between PNA+ and PNA– months had similar
453 geographical patterns, with increases in concentrations in a large fraction of the
454 eastern U.S. and over a belt region along the Rocky Mountain in the western U.S..
455 The increases in concentrations of NO_3^- and NH_4^+ over the eastern U.S. in PNA+
456 months relative to PNA– months agreed very well with those seen in observations
457 (Fig. 3). The differences in concentrations of SO_4^{2-}, NO_3^- and NH_4^+ in the eastern U.S.
458 between the PNA+ and PNA– months were 0.2 μg m^{-3} (4.0%), 0.4 μg m^{-3} (33.5%),
459 and 0.2 μg m^{-3} (13.2%), respectively (Table 2).
460 The differences in concentrations of OC and BC between PNA+ and PNA–
461 months had similar geographical patterns, with large increases in concentrations over
462 and near the eastern Midwest and the region from northwestern U.S. to Texas. The
463 maximum differences reached 0.2–0.4 μg m^{-3} (10–20%) and 0.1–0.2 μg m^{-3} (20–
464 30%) in Illinois, Indiana and Ohio for OC and BC, respectively. The magnitudes of the
465 differences in OC and BC were statistically significant but were smaller than the
466 observations (Tables 1 and 2). The absolute differences in OC were less than 0.1 μg
467 m^{-3} in the western, eastern and whole of U.S due to the underestimation of OC in the
468 simulation.
469 In summary, model results agreed with observations in that the concentrations of
470 all aerosol species of SO_4^{2-}, NO_3^-, NH_4^+, BC, and OC averaged over the U.S. were
471 higher in PNA+ months than in PNA– months. Relative to the PNA– months, the

472 average concentration of $PM_{2.5}$ over the U.S. was higher by about 8.7% (12.2%)
473 based on observed (simulated) concentrations. Furthermore, simulated geographical
474 patterns of the differences in $PM_{2.5}$ and each aerosol species between the PNA+ and
475 PNA– months were similar to those seen in observations, with the largest increases in
476 aerosol concentrations in PNA+ months over and near the eastern Midwest.
477
478 **5 Mechanisms for the impact of PNA on aerosol concentrations**
479 **5.1 The impact of PNA on transboundary transport of aerosols**
480 The transboundary transport of pollutants to and from the U.S. depends largely on
481 winds in the free troposphere (Liang et al. 2004). Figure 6 shows the horizontal winds
482 at 700 hPa averaged over the winter months of NDJFM of 1986–2006 and the
483 corresponding differences between PNA+ and PNA– months on the basis of the
484 GEOS-4 meteorological fields. Strong westerlies prevailed over the U.S. in wintertime
485 (Fig. 6a). Relative to the PNA– months, anomalous northeasterlies occurred over a
486 large fraction of U.S. in the PNA+ months. Anomalous anti-cyclonic circulation
487 occurred near the northwestern U.S. and anomalous cyclonic circulation occurred
488 near the southeastern U.S. (Fig. 6b), corresponding to the large positive and negative
489 differences in geopotential height in these two regions (see auxiliary Fig. S1),
490 respectively.
491 We also calculate mass fluxes of $PM_{2.5}$ at the four lateral boundaries (from the
492 surface to 100 hPa) of the U. S. for different PNA phases (Table 3). The domain of the
493 box to represent the U. S. is (75–120°W, 28–49°N), as shown in Fig. 6b. For $PM_{2.5}$ in
494 wintertime, the inflow from the west boundary and the outflow from the east boundary
495 had the largest absolute values (Table 3). Relative to the PNA– months, the inflow
496 from the west boundary and the outflow from the east boundary in PNA+ months

497 exhibited reductions of 17.1 kg s^{-1} and 12.8 kg s^{-1}, respectively (Table 3). The inflow
498 flux from south boundary decreased by 19.3 kg s^{-1}, and the inflow flux from north
499 boundary increased by 37.6 kg s^{-1}, leading to a net increase of inflow flux of 14.0 kg
500 s^{-1} in PNA+ months. Therefore, the transboundary transport has an overall effect of
501 increasing $PM_{2.5}$ aerosols in the U.S. in PNA+ months relative to PNA– months. The
502 relative change in net flux was 11.4% ((PNA+ minus PNA–)×100%/PNA–) (Table 3),
503 coinciding well with the enhancement of 12.2% in surface-layer $PM_{2.5}$ concentration
504 averaged over the U.S. (Table 2). Note that because the GEOS-Chem model
505 underestimates $PM_{2.5}$ concentrations in the western U.S. (Fig. 4b), the net outflow
506 flux from the selected box might have been underestimated, but this should not
507 compromise our conclusions about the differences in net flux between PNA+ and
508 PNA– phases.

509 **5.2 Local changes in aerosol concentrations caused by the PNA**

510 The PNA pattern is also associated with variations in meteorological variables such
511 as temperature (Leathers et al. 1991; Konrad II 1998; Notaro et al. 2006; Knight et al.
512 2008; Liu et al. 2015; Ning and Bradley 2014, 2015), precipitation (Leathers et al.
513 1991; Henderson and Robinson 1994; Coleman and Rogers 2003; Notaro et al. 2006;
514 Archambault et al. 2008; Myoung and Deng 2009; Ning and Bradley 2014, 2015;
515 Wise et al. 2015) and humidity (Sheridan 2003; Coleman and Rogers 2003; Knight et
516 al. 2008) in U.S.，which are expected to influence aerosol concentrations within the
517 U.S. through chemical reactions, transport, and deposition.

518 Figure 7 shows the composite differences, between the PNA+ and PNA– months,
519 in surface air temperature (T), precipitation rate (PR), relative humidity (RH), surface
520 wind speed (WS), and planetary boundary layer height (PBLH), based on the
521 reanalyzed GEOS-4 datasets. Relative to PNA– months, temperatures were higher

522 by 1–3 K over the northwestern U.S. and lower by 1–4 K in the southeastern region.
523 Such geographic distributions of temperature anomalies were attributed to the
524 maritime warm air in the northwestern U.S. accompanied by the enhanced
525 tropospheric geopotential height in North America (Leathers et al. 1991; Sheridan
526 2003; Liu et al. 2015; Ning and Bradley 2015) (see also auxiliary Fig. 1d) and the
527 more frequent outbreak of cold air in southeastern U.S. accompanied by the
528 depressed geopotential height (Konrad II 1998; Liu et al. 2015) (see also auxiliary Fig.
529 1d). The differences in precipitation between PNA+ and PNA– months reached –1.6
530 to –2.4 mm day^{-1} (–32 to –48%) over and near the eastern Midwest, –2.4 to –3.2 mm
531 day^{-1} (–48 to –64%) in the northwestern U.S., and 1.6–2.4 mm day^{-1} (16–32%) in the
532 southeastern U.S.. These effects of PNA on precipitation were similar to those
533 obtained from wintertime station data by Leathers et al. (1991), Coleman and Rogers
534 (2003) and Wise et al. (2015). With respect to RH, the values in the eastern U.S. were
535 generally lower in the PNA+ months than in PNA– months, as a result of the reduced
536 moisture flux from the Gulf of Mexico to the eastern U.S. (Coleman and Rogers 2003),
537 where RH showed maximum reduction of –3 to –9%. The enhancement of RH of up
538 to 6–9% in Texas, Oklahoma and New Mexico was due to the anomalous easterlies
539 over the south central U.S. (see Fig. 7), which diminished the influence of the dry air
540 from the deserts of the southwestern U.S. and northwestern Mexico in PNA+ months
541 (Sheridan 2003). The surface WS showed reductions in PNA+ months relative to
542 PNA– months in two regions, one was the belt region along the Rocky Mountain from
543 the northwestern U.S. to Texas (with the maximum reductions of 1.5–2.0 m s^{-1} (48–
544 64%)) and the other region, with a northeast-southwest orientation, was from Ohio to
545 Louisiana (with maximum reductions of 0.5–1.0 m s^{-1} (16–32%)). The differences in
546 PBLH between PNA+ and PNA– months were statistically significant in the western

547 U.S. and in the belt region from the northeastern U.S. to the eastern Midwest, with the
548 maximum reductions in PBLH of 75–100 m (15–20%) and 75–100 m (10–15%),
549 respectively.

550 The comparisons of Fig. 5b with Fig. 7a indicate that the increases in $PM_{2.5}$
551 concentrations over and near the eastern Midwest in PNA+ months relative to the
552 PNA– months can be attributed to the decreases in PR, WS and PBLH in these
553 locations, since the changes in these three variables depressed wet deposition, local
554 horizontal diffusion, and vertical diffusion of the surface aerosols, respectively. The
555 increases in SO_4^{2-} in the western U.S. (Fig. 5b) corresponded to the decreases in PR
556 and PBLH and the increased temperature. The increases in temperature enhance
557 chemical reaction rates (Aw and Kleeman 2003; Dawson et al. 2007; Kleeman 2008).
558 In the eastern U.S., although PR, WS, and PBLH decreased over and near the
559 eastern Midwest, the cooling in the eastern U.S. might have offset the effects by PR,
560 WS, and PBLH, inducing practically no changes in SO_4^{2-} in the eastern U.S.. The
561 large increases in NO_3^- and NH_4^+ in the southeastern U.S. (Fig. 5b) can be attributed
562 to the reduced surface temperature, which was favorable to the wintertime formation
563 of NO_3^- and NH_4^+ (Dawson et al. 2007). The differences in concentrations of OC and
564 BC between PNA+ and PNA– corresponded well with the reduced PR, WS and
565 PBLH.

566 In order to quantify the impacts of anomalies in meteorological parameters driven
567 by PNA on concentrations of different aerosol species, the pattern correlation
568 coefficients (PCC, http://glossary.ametsoc.org/wiki/Pattern_correlation) are
569 calculated and shown in Table 4. These pattern correlation coefficients denote the
570 relationship between the geographical distribution of anomalies of each of T, PR, RH,
571 WS, and PBLH (Fig. 7b) and that of the differences in concentration of each aerosol

572 species between PNA+ and PNA– months (Fig. 5c). As shown in Table 4, over the
573 whole U.S., the PNA influenced SO_4^{2-} concentrations mainly through changes PBLH,
574 PR, and T, with the highest PCC values of –0.43, –0.38, and +0.26, respectively. For
575 NO_3^-, the PNA-induced variations in temperature had a strong negative correlation
576 (PCC=–0.59) with the PNA-induced differences in concentrations, indicating that
577 surface temperature was the dominant meteorological factor to influence NO_3^-
578 concentrations. For NH_4^+, OC, and BC, PR and PBLH were the two variables that had
579 the largest negative PCC values (Table 4). Note that PBLH was the most important
580 meteorological variable for SO_4^{2-}, NH_4^+, OC and BC, which contributed to the high
581 correlation between PBLH and $PM_{2.5}$.
582
583 **6 Conclusions**
584 This study examined the impacts of monthly variation in the PNA phase on wintertime
585 surface-layer aerosol concentrations in the U.S. by the analyses of EPA-AQS
586 observations over 1999–2013 and model results for 1986–2006 from the global
587 chemical transport model GEOS-Chem.
588 The composite analyses on the EPA-AQS observations showed that the average
589 concentrations of $PM_{2.5}$, SO_4^{2-}, NO_3^-, NH_4^+, OC, and BC aerosols over the U.S. were
590 higher in the PNA+ months than in the PNA– months by 1.0 μg m^{-3} (8.7%), 0.01 μg
591 m^{-3} (0.5%), 0.3 μg m^{-3} (29.1%), 0.1 μg m^{-3} (11.9%), 0.6 μg m^{-3} (13.5%), and 0.2 μg
592 m^{-3} (27.8%), respectively. Regionally, the observed $PM_{2.5}$ concentrations were higher
593 by 3–5 μg m^{-3} (40–80%) over the Midwest, and by 7–9 μg m^{-3} (80–100%) around the
594 Salt Lake, as the concentrations in PNA+ months were compared to those in PNA–
595 months.

596 The impacts of PNA phase on aerosol concentrations were reproduced fairly well
597 by the GEOS-Chem simulation with fixed anthropogenic emissions (the variations of
598 aerosols concentrations were driven by changes in meteorological fields alone).
599 Concentrations of SO_4^{2-}, NO_3^-, NH_4^+, BC, and OC averaged over the U.S. were
600 simulated to be higher in the PNA+ months than in PNA– months. The average
601 concentration of $PM_{2.5}$ over the U.S. was simulated to be 12.2% higher in the PNA+
602 months relative to the PNA– months, in close agreement with the observations.
603 Simulated geographical patterns of the differences in $PM_{2.5}$ and each aerosol species
604 between the PNA+ and PNA– months were similar to those seen in observations. The
605 largest increases in aerosol concentrations in the PNA+ months were simulated to be
606 over and near the eastern Midwest, but the model results showed small PNA-induced
607 changes in aerosol concentrations in the western U.S..
608 The mechanisms for the impacts of PNA on aerosol concentrations were
609 examined. The transboundary transport was found to have an overall effect of
610 increasing $PM_{2.5}$ aerosols in the U.S. in the PNA+ months relative to PNA– months.
611 Compared to the PNA– months, anomalous northeasterlies occurred over a large
612 fraction of U.S., which led to a net increase in inflow flux of $PM_{2.5}$ of 14.0 Kg s^{-1} in
613 PNA+ months. Regionally within the U.S., the PNA influenced aerosol concentrations
614 through changes in precipitation rate (PR), planetary boundary layer height (PBLH),
615 surface wind speed (WS), surface air temperature (T) and relative humidity (RH), as
616 represented by the pattern correlation coefficients (PCCs). The PNA influenced SO_4^{2-}
617 concentration mainly through changes PBLH, PR, and T, with the highest PCC values
618 of –0.43, –0.38, and +0.26, respectively. For NO_3^-, the PNA-induced variations in
619 temperature had a strong negative correlation (PCC=–0.59) with the PNA-induced
620 differences in concentrations. For NH_4^+, OC, and BC, PR and PBLH were the two

621 variables that had the largest negative PCC values. Because PBLH was the most
622 important meteorological variable for SO_4^{2-}, NH_4^+, OC and BC, which led to a high
623 correlation between PBLH and $PM_{2.5}$.

624 Conclusions from this study have important implications for air quality in the U.S..
625 Leathers and Palechi (1992) showed that the PNAI were generally low in 1947–1957
626 but consistently high in 1958–1987. The PNAI during 1948–2010 exhibited an
627 increasing trend for positive phases and a decreasing trend for negative phases (Liu
628 et al. 2015; Ning et al. 2015; http://research.jisao.washington.edu/data_sets/pna/#djf),
629 indicating that wintertime particulate matter pollution in most areas of U.S.
630 deteriorated due to variations in PNA phase alone. Climate models projected that
631 positive PNA phases would increase in the future because of the global warming
632 (Kachi and Nitta, 1997; Müller and Roeckner 2008; Zhou 2014). Therefore, the trend
633 in PNA pattern underlies the necessity of strict emission reduction strategies for
634 greenhouse gases, aerosols, and aerosol precursors.
635
636
637 *Acknowledgements.* This work was supported by the National Basic Research
638 Program of China (973 program, Grant 2014CB441202), the Strategic Priority
639 Research Program of the Chinese Academy of Sciences Strategic Priority Research
640 Program Grant No. XDA05100503, and the National Natural Science Foundation of
641 China under grants 91544219, 41475137, and 41321064.
642

References

Alexander, B., Park, R.J., Jacob, D.J., Li, Q.B., Yantosca, R.M., Savarino, J., Lee, C.C.W., Thiemens, M.H.: Sulfate formation in sea-salt aerosols: Constraints from oxygen isotopes, J. Geophys. Res., 110(D10), D10307, doi:10.1029/2004JD005659, 2005.

Allen, R. J., Landuyt, W. and Rumbold, S. T.: An increase in aerosol burden and radiative effects in a warmer world, Nat. Clim. Chang., (OCTOBER), doi:10.1038/nclimate2827, 2015.

Alston, E. J., Sokolik, I. N. and Kalashnikova, O. V.: Characterization of atmospheric aerosol in the US Southeast from ground- and space-based measurements over the past decade, Atmos. Meas. Tech., 5(7), 1667–1682, doi:10.5194/amt-5-1667-2012, 2012.

Archambault, H. M., Bosart, L. F., Keyser, D. and Aiyyer, A. R.: Influence of Large-Scale Flow Regimes on Cool-Season Precipitation in the Northeastern United States, Mon. Weather Rev., 136(8), 2945–2963, doi:10.1175/2007MWR2308.1, 2008.

Athanasiadis, P. J. and Ambaum, M. H. P.: Linear Contributions of Different Time Scales to Teleconnectivity, J. Clim., 22(13), 3720–3728, doi:10.1175/2009JCLI2707.1, 2009.

Aw, J. and Kleeman, M. J.: Evaluating the first-order effect of intraannual temperature variability on urban air pollution, J. Geophys. Res., 108(D12), 4365, doi:10.1029/2002JD002688, 2003.

Bauer, S. E., Koch, D., Unger, N., Metzger, S. M., Shindell, D. T. and Streets, D. G.: Nitrate aerosols today and in 2030: a global simulation including aerosols and tropospheric ozone, Atmos. Chem. Phys., 7(19), 5043–5059, doi:10.5194/acp-7-5043-2007, 2007.

Bey, I., Jacob, D. J., Yantosca, R. M., Logan, J. a., Field, B. D., Fiore, A. M., Li, Q., Liu, H. Y., Mickley, L. J. and Schultz, M. G.: Global modeling of tropospheric chemistry with assimilated meteorology: Model description and evaluation, J. Geophys. Res., 106(D19), 23073, doi:10.1029/2001JD000807, 2001.

Blackmon, M. L., Lee, Y.-H. and Wallace, J. M.: Horizontal Structure of 500 mb Height Fluctuations with Long, Intermediate and Short Time Scales, J. Atmos. Sci., 41(6), 961–980, doi:10.1175/1520-0469(1984)041<0961:HSOMHF>2.0.CO;2, 1984.

Cakmur, R. V., Miller, R. L. and Tegen, I.: A comparison of seasonal and interannual variability of soil dust aerosols over the Atlantic Ocean as inferred by the TOMS AI and AVHRR AOT retrievals, J. Geophys. Res., 106(D16), 18287, doi:10.1029/2000JD900525, 2001.

Chen, J., Vaughan, J., Avise, J., O'Neill, S. and Lamb, B.: Enhancement and evaluation of the AIRPACT ozone and $PM_{2.5}$ forecast system for the Pacific Northwest, J. Geophys. Res. Atmos., 113(14), 1–20, doi:10.1029/2007JD009554, 2008.

Coleman, J. S. M. and Rogers, J. C.: Ohio River Valley Winter Moisture Conditions Associated with the Pacific–North American Teleconnection Pattern, J. Clim.,

16(6), 969–981, doi:10.1175/1520-0442(2003)016<0969:ORVWMC>2.0.CO;2, 2003.

Dawson, J. P., Adams, P. J. and Pandis, S. N.: Sensitivity of $PM_{2.5}$ to climate in the Eastern US: a modeling case study, Atmos. Chem. Phys., 7(16), 4295–4309, doi:10.5194/acp-7-4295-2007, 2007.

Day, M. C. and Pandis, S. N.: Predicted changes in summertime organic aerosol concentrations due to increased temperatures, Atmos. Environ., 45(36), 6546–6556, doi:10.1016/j.atmosenv.2011.08.028, 2011.

Di Pierro, M., Jaeglé, L. and Anderson, T. L.: Satellite observations of aerosol transport from East Asia to the Arctic: three case studies, Atmos. Chem. Phys., 11(5), 2225–2243, doi:10.5194/acp-11-2225-2011, 2011.

Drury, E., Jacob, D. J., Spurr, R. J. D., Wang, J., Shinozuka, Y., Anderson, B. E., Clarke, A. D., Dibb, J., McNaughton, C. and Weber, R.: Synthesis of satellite (MODIS), aircraft (ICARTT), and surface (IMPROVE, EPA-AQS, AERONET) aerosol observations over eastern North America to improve MODIS aerosol retrievals and constrain surface aerosol concentrations and sources, J. Geophys. Res., 115(D14), D14204, doi:10.1029/2009JD012629, 2010.

Duncan, B. N., Martin, R. V., Staudt, A. C., Yevich, R. and Logan, J. A.: Interannual and seasonal variability of biomass burning emissions constrained by satellite observations, J. Geophys. Res., 108(D2), 4100, doi:10.1029/2002JD002378, 2003.

Dutkiewicz, V. A., Das, M. and Husain, L.: The relationship between regional SO2 emissions and downwind aerosol sulfate concentrations in the northeastern US, Atmos. Environ., 34(11), 1821–1832, doi:10.1016/S1352-2310(99)00334-9, 2000.

Fairlie, D. T., Jacob, D. J. and Park, R. J.: The impact of transpacific transport of mineral dust in the United States, Atmos. Environ., 41(6), 1251–1266, doi:10.1016/j.atmosenv.2006.09.048, 2007.

Feldstein, S. B.: Fundamental mechanisms of the growth and decay of the PNA teleconnection pattern, Q. J. R. Meteorol. Soc., 128(581), 775–796, doi:10.1256/0035900021643683, 2002.

Feldstein, S. B.: The dynamics of NAO teleconnection pattern growth and decay, Q. J. R. Meteorol. Soc., 129(589), 901–924, doi:10.1256/qj.02.76, 2003.

Fu, T.-M., Jacob, D. J. and Heald, C. L.: Aqueous-phase reactive uptake of dicarbonyls as a source of organic aerosol over eastern North America, Atmos. Environ., 43(10), 1814–1822, doi:10.1016/j.atmosenv.2008.12.029, 2009.

Generoso, S., Bréon, F.-M., Balkanski, Y., Boucher, O. and Schulz, M.: Improving the seasonal cycle and interannual variations of biomass burning aerosol sources, Atmos. Chem. Phys., 3(4), 1211–1222, doi:10.5194/acp-3-1211-2003, 2003.

Giglio, L., van der Werf, G. R., Randerson, J. T., Collatz, G. J. and Kasibhatla, P.: Global estimation of burned area using MODIS active fire observations, Atmos. Chem. Phys., 6(4), 957–974, doi:10.5194/acp-6-957-2006, 2006.

Gong, S. L., Zhang, X. Y., Zhao, T. L., Zhang, X. B., Barrie, L. A., McKendry, I. G. and Zhao, C. S.: A Simulated Climatology of Asian Dust Aerosol and Its Trans-Pacific

731 Transport. Part II: Interannual Variability and Climate Connections, J. Clim.,
732 19(1), 104–122, doi:10.1175/JCLI3606.1, 2006.

733 Guenther, A., Karl, T., Harley, P., Wiedinmyer, C., Palmer, P. I. and Geron, C.:
734 Estimates of global terrestrial isoprene emissions using MEGAN (Model of
735 Emissions of Gases and Aerosols from Nature), Atmos Chem Phys 6:3181-3210.
736 doi: 10.5194/acp-6-3181-2006, 2006.

737 Hack, J. J.: Parameterization of moist convection in the National Center for
738 Atmospheric Research community climate model (CCM2), J. Geophys. Res.,
739 99(D3), 5551, doi:10.1029/93JD03478, 1994.

740 Hand, J. L., Schichtel, B. A., Malm, W. C. and Pitchford, M. L.: Particulate sulfate ion
741 concentration and SO_2 emission trends in the United States from the early 1990s
742 through 2010, Atmos. Chem. Phys., 12(21), 10353–10365,
743 doi:10.5194/acp-12-10353-2012, 2012a.

744 Hand, J. L., Schichtel, B. A., Pitchford, M., Malm, W. C. and Frank, N. H.: Seasonal
745 composition of remote and urban fine particulate matter in the United States, J.
746 Geophys. Res., 117(D5), D05209, doi:10.1029/2011JD017122, 2012b.

747 Hand, J. L., Schichtel, B. A., Malm, W. C., Pitchford, M. and Frank, N. H.: Spatial and
748 seasonal patterns in urban influence on regional concentrations of speciated
749 aerosols across the United States, J. Geophys. Res. Atmos., 119, 12832–
750 12849, doi:10.1002/2014JD022328.Received, 2014.

751 Heald, C. L., Jacob, D. J., Park, R. J., Alexander, B., Fairlie, T. D., Yantosca, R. M. and
752 Chu, D. A.: Transpacific transport of Asian anthropogenic aerosols and its impact
753 on surface air quality in the United States, J. Geophys. Res. D Atmos., 111, 1–13,
754 doi:10.1029/2005JD006847, 2006.

755 Heald, C. L., Henze, D. K., Horowitz, L. W., Feddema, J., Lamarque, J.-F., Guenther,
756 A., Hess, P. G., Vitt, F., Seinfeld, J. H., Goldstein, A. H. and Fung, I.: Predicted
757 change in global secondary organic aerosol concentrations in response to future
758 climate, emissions, and land use change, J. Geophys. Res. Atmos., 113(D5),
759 D05211, doi:10.1029/2007JD009092, 2008.

760 Henderson, K. G. and Robinson, P. J.: Relationships between the pacific/north
761 american teleconnection patterns and precipitation events in the south-eastern
762 USA, Int. J. Climatol., 14(3), 307–323, doi:10.1002/joc.3370140305, 1994.

763 IPCC: Climate Change 2013 The Physical Science Basis: Working Group I
764 Contribution to the Fifth Assessment Report of the Intergovernmental Panel on
765 Climate Change, 1st ed., Cambridge University Press, New York. [online]
766 Available from:
767 http://www.climatechange2013.org/images/report/WG1AR5_ALL_FINAL.pdf"
768 The last access date was November 20, 2015.

769 Jacob, D. J. and Winner, D. A.: Effect of climate change on air quality, Atmos. Environ.,
770 43(1), 51–63, doi:10.1016/j.atmosenv.2008.09.051, 2009.

771 Jaffe, D., Tamura, S. and Harris, J.: Seasonal cycle and composition of background
772 fine particles along the west coast of the US, Atmos. Environ., 39(2), 297–306,
773 doi:10.1016/j.atmosenv.2004.09.016, 2005.

774 Jerez, S., Jimenez-Guerrero, P., Montávez, J. P. and Trigo, R. M.: Impact of the North
775 Atlantic Oscillation on European aerosol ground levels through local processes:

776 a seasonal model-based assessment using fixed anthropogenic emissions,
777 Atmos. Chem. Phys., 13(22), 11195–11207, doi:10.5194/acp-13-11195-2013,
778 2013.

779 Juda-Rezler, K., Reizer, M., Huszar, P., Krüger, B., Zanis, P., Syrakov, D., Katragkou,
780 E., Trapp, W., Melas, D., Chervenkov, H., Tegoulias, I. and Halenka, T.:
781 Modelling the effects of climate change on air quality over Central and Eastern
782 Europe: concept, evaluation and projections, Clim. Res., 53(3), 179–203,
783 doi:10.3354/cr01072, 2012.

784 Kachi, M. and Nitta, T.: Decadal variations of the global atmosphere-ocean system, J.
785 Meteorol. Soc. Japan, 75(3), 657–675, 1997.

786 Kleeman, M. J.: A preliminary assessment of the sensitivity of air quality in California to
787 global change, Clim. Change, 87(1), 273–292, doi:10.1007/s10584-007-9351-3,
788 2008.

789 Knight, D. B., Davis, R. E., Sheridan, S. C., Hondula, D. M., Sitka, L. J., Deaton, M.,
790 Lee, T. R., Gawtry, S. D., Stenger, P. J., Mazzei, F. and Kenny, B. P.: Increasing
791 frequencies of warm and humid air masses over the conterminous United States
792 from 1948 to 2005, Geophys. Res. Lett., 35(10), L10702,
793 doi:10.1029/2008GL033697

794 Konrad II, C. E.: Persistent planetary scale circulation patterns and their relationship
795 with cold air outbreak activity over the Eastern United States, Int. J. Climatol.,
796 18(11), 1209–1221,
797 doi:10.1002/(SICI)1097-0088(199809)18:11<1209::AID-JOC301>3.0.CO;2-K,
798 1998.

799 Lam, Y. F., Fu, J. S., Wu, S. and Mickley, L. J.: Impacts of future climate change and
800 effects of biogenic emissions on surface ozone and particulate matter
801 concentrations in the United States, Atmos. Chem. Phys., 11(10), 4789–4806,
802 doi:10.5194/acp-11-4789-2011, 2011.

803 Leathers, D. J. and Palecki, M. A.: The Pacific/North American Teleconnection Pattern
804 and United States Climate. Part II: Temporal Characteristics and Index
805 Specification, J. Clim., 5(7), 707–716,
806 doi:10.1175/1520-0442(1992)005<0707:TPATPA>2.0.CO;2, 1992.

807 Leathers, D. J., Yarnal, B. and Palecki, M. A.: The Pacific/North American
808 Teleconnection Pattern and United States Climate. Part I: Regional Temperature
809 and Precipitation Associations, J. Clim., 4(5), 517–528,
810 doi:10.1175/1520-0442(1991)004<0517:TPATPA>2.0.CO;2, 1991.

811 Leibensperger, E. M., Mickley, L. J., Jacob, D. J. and Barrett, S. R. H.: Intercontinental
812 influence of NO_x and CO emissions on particulate matter air quality, Atmos.
813 Environ., 45(19), 3318–3324, doi:10.1016/j.atmosenv.2011.02.023, 2011.

814 Li, J., Carlson, B. E. and Lacis, A. A.: Application of spectral analysis techniques in the
815 intercomparison of aerosol data: 1. An EOF approach to analyze the
816 spatial-temporal variability of aerosol optical depth using multiple remote sensing
817 data sets, J. Geophys. Res. Atmos., 118(15), 8640–8648,
818 doi:10.1002/jgrd.50686, 2013.

819 Liang, Q., Jaeglé, L., Jaffe, D. A., Weiss-Penzias, P., Heckman, A. and Snow, J. A.:
820 Long-range transport of Asian pollution to the northeast Pacific: Seasonal

821 variations and transport pathways of carbon monoxide, J. Geophys. Res. D
822 Atmos., 109, 1–16, doi:10.1029/2003JD004402, 2004.

823 Liang, Q., Jaeglé, L. and Wallace, J. M.: Meteorological indices for Asian outflow and
824 transpacific transport on daily to interannual timescales, J. Geophys. Res.,
825 110(D18), D18308, doi:10.1029/2005JD005788, 2005.

826 Liao, H., Chen, W. T. and Seinfeld, J. H.: Role of climate change in global predictions
827 of future tropospheric ozone and aerosols, J. Geophys. Res. Atmos., 111, 1–18,
828 doi:10.1029/2005JD006852, 2006.

829 Liao, H., Henze, D. K., Seinfeld, J. H., Wu, S. and Mickley, L. J.: Biogenic secondary
830 organic aerosol over the United States: Comparison of climatological simulations
831 with observations, J. Geophys. Res., 112(D6), D06201,
832 doi:10.1029/2006JD007813, 2007.

833 Lin, S.-J. and Rood, R. B.: Multidimensional Flux-Form Semi-Lagrangian Transport
834 Schemes, Mon. Weather Rev., 124(9), 2046–2070,
835 doi:10.1175/1520-0493(1996)124<2046:MFFSLT>2.0.CO;2, 1996.

836 Liu, H.-Y., Jacob, D. J., Bey, I. and Yantosca, R. M.: Constraints Pb-210 and Be-7 on
837 Wet Deposition and Transport in a Global Three-Dimensional Chemical Tracer
838 Model Driven by Assimilated Meteorological Fields, J. Geophys. Res. Atmos.,
839 106(Dll), doi:10.1029/2000JD900839, 2001.

840 Liu, Y., Park, R. J., Jacob, D. J., Li, Q., Kilaru, V. and Sarnat, J. A.: Mapping annual
841 mean ground-level $PM_{2.5}$ concentrations using Multiangle Imaging
842 Spectroradiometer aerosol optical thickness over the contiguous United States, J.
843 Geophys. Res., 109(D22), D22206, doi:10.1029/2004JD005025, 2004.

844 Liu, Y., Liu, J. and Tao, S.: Interannual variability of summertime aerosol optical depth
845 over East Asia during 2000–2011: a potential influence from El Niño Southern
846 Oscillation, Environ. Res. Lett., 8(4), 044034,
847 doi:10.1088/1748-9326/8/4/044034, 2013.

848 Liu, Z., Jian, Z., Yoshimura, K., Buenning, N. H., Poulsen, C. J. and Bowen, G. J.:
849 Recent contrasting winter temperature changes over North America linked to
850 enhanced positive Pacific-North American pattern, Geophys. Res. Lett., 42, 1–8,
851 doi:10.1002/2015GL065656, 2015.

852 Mahowald, N., Luo, C., del Corral, J., Zender, C.S.: Interannual variability in
853 atmospheric mineral aerosols from a 22-year model simulation and
854 observational data, J. Geophys. Res., 108(D12), 4352,
855 doi:10.1029/2002JD002821, 2003.

856 Malm, W. C.: Spatial and monthly trends in speciated fine particle concentration in the
857 United States, J. Geophys. Res., 109(D3), D03306, doi:10.1029/2003JD003739,
858 2004.

859 Malm, W. C., Schichtel, B. A. and Pitchford, M. L.: Uncertainties in $PM_{2.5}$ Gravimetric
860 and Speciation Measurements and What We Can Learn from Them, J. Air Waste
861 Manage. Assoc., 61(11), 1131–1149, doi:10.1080/10473289.2011.603998,
862 2011.

863 Markakis, K., Valari, M., Perrussel, O., Sanchez, O. and Honore, C.: Climate-forced
864 air-quality modeling at the urban scale: sensitivity to model resolution, emissions

865 and meteorology, Atmos. Chem. Phys., 15(13), 7703–7723,
866 doi:10.5194/acp-15-7703-2015, 2015.

867 Megaritis, a. G., Fountoukis, C., Charalampidis, P. E., Denier van der Gon, H. a. C.,
868 Pilinis, C. and Pandis, S. N.: Linking climate and air quality over Europe: effects
869 of meteorology on $PM_{2.5}$ concentrations, Atmos. Chem. Phys., 14(18), 10283–
870 10298, doi:10.5194/acp-14-10283-2014, 2014.

871 Mijling, B., van der A, R. J. and Zhang, Q.: Regional nitrogen oxides emission trends in
872 East Asia observed from space, Atmos. Chem. Phys., 13, 12003-12012, doi:
873 10.5194/acp-13-12003-2013, 2013.

874 Moulin, C. and Lambert, C. E., Dulac, F., Dayan, U.: Control of atmospheric export of
875 dust from North Africa by the North Atlantic Oscillation, Nature, 387(June), 691–
876 694, 1997.

877 Mu, Q. and Liao, H.: Simulation of the interannual variations of aerosols in China: role
878 of variations in meteorological parameters, Atmos. Chem. Phys., 14, 11177–
879 11219, doi:10.5194/acp-14-9597-2014, 2014.

880 Müller, W. A. and Roeckner, E.: ENSO teleconnections in projections of future climate
881 in ECHAM5/MPI-OM, Clim. Dyn., 31(5), 533–549,
882 doi:10.1007/s00382-007-0357-3, 2008.

883 Murray, L. T., Jacob, D. J., Logan, J. A., Hudman, R. C. and Koshak, W. J.: Optimized
884 regional and interannual variability of lightning in a global chemical transport
885 model constrained by LIS/OTD satellite data, J. Geophys. Res. Atmos.,
886 117(D20), D20307, doi:10.1029/2012JD017934, 2012.

887 Myoung, B. and Deng, Y.: Interannual Variability of the Cyclonic Activity along the U.S.
888 Pacific Coast: Influences on the Characteristics of Winter Precipitation in the
889 Western United States, J. Clim., 22(21), 5732–5747,
890 doi:10.1175/2009JCLI2889.1, 2009.

891 Ning, L. and Bradley, R. S.: Winter precipitation variability and corresponding
892 teleconnections over the northeastern United States, J. Geophys. Res. Atmos.,
893 119(13), 7931–7945, doi:10.1002/2014JD021591, 2014.

894 Ning, L. and Bradley, R. S.: Winter Climate Extremes over the Northeastern United
895 States and Southeastern Canada and Teleconnections with Large-Scale Modes
896 of Climate Variability, J. Clim., 28(6), 2475–2493,
897 doi:10.1175/JCLI-D-13-00750.1, 2015.

898 Notaro, M., Wang, W.-C. and Gong, W.: Model and Observational Analysis of the
899 Northeast U.S. Regional Climate and Its Relationship to the PNA and NAO
900 Patterns during Early Winter, Mon. Weather Rev., 134(11), 3479–3505,
901 doi:10.1175/MWR3234.1, 2006.

902 Park, R. J., Jacob, D. J., Chin, M., Martin, R. V.: Sources of carbonaceous aerosols
903 over the United States and implications for natural visibility, J. Geophys. Res.,
904 108(D12), 4355, doi:10.1029/2002JD003190, 2003.

905 Park, R. J., Jacob, D. J., Field, B. D., Yantosca, R. M., Chin, M.: Natural and
906 transboundary pollution influences on sulfate-nitrate-ammonium aerosols in the
907 United States: Implications for policy, J. Geophys. Res., 109(D15), D15204,
908 doi:10.1029/2003JD004473, 2004.

909 Park, R. J., Jacob, D. J., Palmer, P. I., Clarke, A. D., Weber, R. J., Zondlo, M. A.,
910 Eisele, F. L., Bandy, A. R., Thornton, D. C., Sachse, G. W. and Bond, T. C.:
911 Export efficiency of black carbon aerosol in continental outflow: Global
912 implications, J. Geophys. Res. Atmos., 110, 1–7, doi:10.1029/2004JD005432,
913 2005.

914 Park, R. J., Jacob, D. J., Kumar, N. and Yantosca, R. M.: Regional visibility statistics in
915 the United States: Natural and transboundary pollution influences, and
916 implications for the Regional Haze Rule, Atmos. Environ., 40(28), 5405–5423,
917 doi:10.1016/j.atmosenv.2006.04.059, 2006.

918 Porter, W. C., Heald, C. L., Cooley, D. and Russell, B.: Investigating the observed
919 sensitivities of air-quality extremes to meteorological drivers via quantile
920 regression, Atmos. Chem. Phys., 15(18), 10349–10366,
921 doi:10.5194/acp-15-10349-2015, 2015.

922 Pye, H. O. T., Liao, H., Wu, S., Mickley, L. J., Jacob, D. J., Henze, D. K. and Seinfeld,
923 J. H.: Effect of changes in climate and emissions on future
924 sulfate-nitrate-ammonium aerosol levels in the United States, J. Geophys. Res.,
925 114(D1), D01205, doi:10.1029/2008JD010701, 2009.

926 Qian, B., Corte-Real, J. and Xu, H.: Is the North Atlantic Oscillation the most important
927 atmospheric pattern for precipitation in Europe?, J. Geophys. Res., 105(D9),
928 11901, doi:10.1029/2000JD900102, 2000.

929 Rattigan, O. V., Felton, H. D., Bae, M.-S., Schwab, J. J. and Demerjian, K. L.:
930 Comparison of long-term $PM_{2.5}$ carbon measurements at an urban and rural
931 location in New York, Atmos. Environ., 45(19), 3228–3236,
932 doi:10.1016/j.atmosenv.2011.03.048, 2011.

933 Redmond, K. T. and Koch, R. W.: Surface Climate and Streamflow Variability in the
934 Western United States and Their Relationship to Large-Scale Circulation Indices,
935 Water Resour. Res., 27(9), 2381–2399, doi:10.1029/91WR00690, 1991.

936 Sauvage, B., Martin, R. V., van Donkelaar, A., Liu, X., Chance, K., Jaeglé, L., Palmer,
937 P. I., Wu, S. and Fu, T.-M.: Remote sensed and in situ constraints on processes
938 affecting tropical tropospheric ozone, Atmos. Chem. Phys., 7(3), 815–838,
939 doi:10.5194/acp-7-815-2007, 2007.

940 Sheridan, S. C.: North American weather-type frequency and teleconnection indices,
941 Int. J. Climatol., 23(1), 27–45, doi:10.1002/joc.863, 2003.

942 Singh, A. and Palazoglu, A.: Climatic variability and its influence on ozone and PM
943 pollution in 6 non-attainment regions in the United States, Atmos. Environ., 51,
944 212–224, doi:10.1016/j.atmosenv.2012.01.020, 2012.

945 Tai, A. P. K., Mickley, L. J., Jacob, D. J., Leibensperger, E. M., Zhang, L., Fisher, J. A.
946 and Pye, H. O. T.: Meteorological modes of variability for fine particulate matter
947 ($PM_{2.5}$) air quality in the United States: implications for $PM_{2.5}$ sensitivity to climate
948 change, Atmos. Chem. Phys., 12(6), 3131–3145,
949 doi:10.5194/acp-12-3131-2012, 2012a.

950 Tai, A. P. K., Mickley, L. J. and Jacob, D. J.: Correlations between fine particulate
951 matter ($PM_{2.5}$) and meteorological variables in the United States: Implications for
952 the sensitivity of $PM_{2.5}$ to climate change, Atmos. Environ., 44(32), 3976–3984,
953 doi:10.1016/j.atmosenv.2010.06.060, 2010.

954 Tai, A. P. K., Mickley, L. J. and Jacob, D. J.: Impact of 2000–2050 climate change on
955 fine particulate matter ($PM_{2.5}$) air quality inferred from a multi-model analysis of
956 meteorological modes, Atmos. Chem. Phys., 12(23), 11329–11337,
957 doi:10.5194/acp-12-11329-2012, 2012b.

958 Unger, N., Shindell, D. T., Koch, D. M., Amann, M., Cofala, J. and Streets, D. G.:
959 Influences of man-made emissions and climate changes on tropospheric ozone,
960 methane, and sulfate at 2030 from a broad range of possible futures, J. Geophys.
961 Res., 111(D12), D12313, doi:10.1029/2005JD006518, 2006.

962 van der Werf, G. R., Randerson, J. T., Giglio, L., Collatz, G. J., Kasibhatla, P. S. and
963 Arellano, A. F.: Interannual variability of global biomass burning emissions from
964 1997 to 2004, Atmos. Chem. Phys, 6, 3423-3441, doi:
965 10.5194/acpd-6-3175-2006, 2006.

966 van Donkelaar, A., Martin, R. V., Park, R. J.: Estimating ground-level $PM_{2.5}$ using
967 aerosol optical depth determined from satellite remote sensing, J. Geophys. Res.,
968 111(D21), D21201, doi:10.1029/2005JD006996, 2006.

969 van Donkelaar, A., Martin, R. V., Park, R. J., Heald, C. L., Fu, T. M., Liao, H. and
970 Guenther, A.: Model evidence for a significant source of secondary organic
971 aerosol from isoprene, Atmos. Environ., 41(6), 1267–1274,
972 doi:10.1016/j.atmosenv.2006.09.051, 2007.

973 van Donkelaar, A., Martin, R. V., Leaitch, W. R., Macdonald, A. M., Walker, T. W.,
974 Streets, D. G., Zhang, Q., Dunlea, E. J., Jimenez, J. L., Dibb, J. E., Huey, L. G.,
975 Weber, R. and Andreae, M. O.: Analysis of aircraft and satellite measurements
976 from the Intercontinental Chemical Transport Experiment (INTEX-B) to quantify
977 long-range transport of East Asian sulfur to Canada, Atmos. Chem. Phys., 8(11),
978 2999–3014, doi:10.5194/acp-8-2999-2008, 2008.

979 Vestreng, V., Myhre, G., Fagerli, H., Reis, S. and Tarrasón, L.: Twenty-five years of
980 continuous sulphur dioxide emission reduction in Europe, Atmos. Chem. Phys.,
981 7(13), 3663–3681, doi:10.5194/acp-7-3663-2007, 2007.

982 Wallace, J. M. and Gutzler, D. S.: Teleconnections in the Geopotential Height Field
983 during the Northern Hemisphere Winter, Mon. Weather Rev., 109(4), 784–812,
984 doi:10.1175/1520-0493(1981)109<0784:TITGHF>2.0.CO;2, 1981.

985 Wang H, Chen H and Liu J: Arctic Sea Ice Decline Intensified Haze Pollution in
986 Eastern China, Atmospheric and Oceanic Science Letters, 8(1), 1–9,
987 doi:10.3878/AOSL20140081, 2015.

988 Wang, Y., Logan, J. A. and Jacob, D. J.: Global simulation of tropospheric O_3
989 -NO_x-hydrocarbon chemistry: 2. Model evaluation and global ozone budget, J.
990 Geophys. Res., 103(D9), 10727, doi:10.1029/98JD00157, 1998.

991 Wesely, M. L.: Parameterization of surface resistances to gaseous dry deposition in
992 regional-scale numerical models, Atmos. Environ., 23(6), 1293–1304,
993 doi:10.1016/0004-6981(89)90153-4, 1989.

994 Wheeler, M. C. and Hendon, H. H.: An all-season real-time multivariate MJO index:
995 Development of an index for monitoring and prediction, Mon. Weather Rev.,
996 132(8), 1917–1932,
997 doi: 10.1175/1520-0493(2004)132<1917:AARMMI>2.0.CO;2,, 2004.

998 Wise, E. K. and Comrie, A. C.: Meteorologically adjusted urban air quality trends in the
999 Southwestern United States, Atmos. Environ., 39(16), 2969–2980,
1000 doi:10.1016/j.atmosenv.2005.01.024, 2005.

1001 Xiao, D., Li, Y., Fan, S., Zhang, R., Sun, J. and Wang, Y.: Plausible influence of
1002 Atlantic Ocean SST anomalies on winter haze in China, Theor. Appl. Climatol.,
1003 doi:10.1007/s00704-014-1297-6, 2014.

1004 Yang, Y., Liao, H. and Lou, S.: Decadal trend and interannual variation of outflow of
1005 aerosols from East Asia: Roles of variations in meteorological parameters and
1006 emissions, Atmos. Environ., 100, 141–153, doi:10.1016/j.atmosenv.2014.11.004,
1007 2015.

1008 Yienger, J. J. and Levy, H.: Empirical model of global soil-biogenic NO_x emissions, J.
1009 Geophys. Res., 100(D6), 11447, doi:10.1029/95JD00370, 1995.

1010 Zhang, G. J. and McFarlane, N. A.: Sensitivity of climate simulations to the
1011 parameterization of cumulus convection in the Canadian climate centre general
1012 circulation model, Atmosphere-Ocean, 33(3), 407–446,
1013 doi:10.1080/07055900.1995.9649539, 1995.

1014 Zhang, L., Jacob, D. J., Knipping, E. M., Kumar, N., Munger, J. W., Carouge, C. C.,
1015 van Donkelaar, A., Wang, Y. X. and Chen, D.: Nitrogen deposition to the United
1016 States: distribution, sources, and processes, Atmos. Chem. Phys., 12(10),
1017 4539–4554, doi:10.5194/acp-12-4539-2012, 2012.

1018 Zhang, L., Kok, J. F., Henze, D. K., Li, Q. and Zhao, C.: Improving simulations of fine
1019 dust surface concentrations over the western United States by optimizing the
1020 particle size distribution, Geophys. Res. Lett., 40(12), 3270–3275,
1021 doi:10.1002/grl.50591, 2013.

1022 Zhou, Z.-Q., Xie, S.-P., Zheng, X.-T., Liu, Q. and Wang, H.: Global Warming–Induced
1023 Changes in El Niño Teleconnections over the North Pacific and North America, J.
1024 Clim., 27(24), 9050–9064, doi:10.1175/JCLI-D-14-00254.1, 2014.

1025 Zhu, J., Liao, H. and Li, J.: Increases in aerosol concentrations over eastern China due
1026 to the decadal-scale weakening of the East Asian summer monsoon, Geophys.
1027 Res. Lett., 39(9), L09809, doi:10.1029/2012GL051428, 2012.

1028

Table 1. The absolute (μg m^{-3}) and relative (%) differences in observed aerosol concentrations between the PNA+ and PNA– months (PNA+ minus PNA–). The observed concentrations are averaged over all the sites in the whole of U.S., in the western U.S., or in the eastern U.S.. See Fig 1 for locations of the sites. The measurements are from the EPA-AQS data. The ** and * indicate the differences that have passed the two-tail student-t test with 95% and 90% significance levels, respectively.

	Whole U.S.	Western U.S.	Eastern U.S
$PM_{2.5}$	1.0 (8.7%)**	1.3 (14.3%)**	0.8 (7.2%)**
SO_4^{2-}	0.01 (0.5%)	0.03 (3.2%)	0.1 (3.7%)
NO_3^-	0.3 (29.1%)**	0.2 (23.8%)**	0.4 (36.5%)**
NH_4^+	0.1 (11.9%)*	0.2 (31.6%)**	0.1 (10.5%)
OC	0.6 (13.5%)**	0.9 (17.7%)**	0.3 (8.0%)**
BC	0.2 (27.8%)**	0.2 (25.0%)**	0.1 (25.2%)**

Table 2. The absolute (μg m^{-3}) and relative (%) differences in simulated aerosol concentrations between the PNA+ and PNA– months (PNA+ minus PNA–). The simulated concentrations are averaged over the whole of U.S., the western U.S. (west of 100°W), or the eastern U.S. (east of 100°W). The concentrations are from the GEOS-Chem simulation for 1986–2006. The ** and * indicate the differences that have passed the two-tail student-t test with 95% and 90% significance levels, respectively.

	Whole U.S.	Western U.S.	Eastern U.S.
$PM_{2.5}$	0.6 (12.2%)**	0.3 (14.0%)**	0.9 (10.8%)**
SO_4^{2-}	0.2 (7.1%)	0.1 (13.5%) **	0.2 (4.0%)
NO_3^-	0.2 (30.3%) **	0.1 (28.5%) **	0.4 (33.5%)**
NH_4^+	0.2 (14.4%)**	0.1 (15.4%)**	0.2 (13.2%)**
OC	0.05 (6.5%)**	0.03 (8.6%)**	0.08 (5.9%)**
BC	0.03 (10.2%)**	0.01 (8.6%)**	0.05 (11.0%)**

1045 **Table 3.** The composite analyses of horizontal mass fluxes (kg s^{-1}) of $PM_{2.5}$ for the
1046 selected box of (75–120°W, 28–49°N, from the surface to 100 hPa) in the PNA+ and
1047 PNA– months of 1986–2006. The positive values at the four boundaries indicate
1048 eastward or northward transport, and negative values indicate westward or
1049 southward transport. The positive (negative) value of net flux indicates the net gain
1050 (loss) of $PM_{2.5}$ in the selected box. All the fluxes are from the GEOS-Chem simulation.

	Boundaries and total	Mass Flux
PNA+	West	89.7
	East	259.3
	South	24.4
	North	–36.2
	Net flux	–109.0
PNA–	West	106.8
	East	272.1
	South	43.7
	North	1.4
	Net flux	–123.0
Diff. (PNA+ minus PNA–)	West	–17.1
	East	–12.8
	South	–19.3
	North	–37.6
	Net flux	14.0

1051

Table 4. The pattern correlation coefficients between the composite differences in aerosol concentrations (Fig. 5c) and the corresponding composite differences in meteorological parameters (Fig. 7b). The * denotes the correlations that have passed the two-tail t-test with 95% confidence level.

	$PM_{2.5}$	SO_4^{2-}	NO_3^-	NH_4^+	OC	BC
T	–0.13	0.26*	–0.59*	–0.22*	0.07	–0.16
PR	–0.44*	–0.38*	0.04	–0.42*	–0.63*	–0.50*
RH	–0.08	–0.05	–0.02	0.12	–0.32*	–0.36*
WS	–0.27*	–0.1	–0.22*	–0.27*	–0.28*	–0.24*
PBLH	–0.61*	–0.43*	–0.32*	–0.61*	–0.60*	–0.55*

Figure Captions

Fig. 1. The locations of EPA-AQS sites with measurements that meet the criteria described in Sect. 2.1 in the text. $PM_{2.5}$ measurements are available for years of 1999–2013 (sites are marked by black dots) and speciated aerosol (SO_4^{2-}, NO_3^-, NH_4^+, BC, and OC) concentrations are available over years of 2000–2013 (sites are marked by red diamonds). The grey solid line defines the western United States (west of 100°W) and eastern United States (east of 100°W).

Fig. 2. (a) PNAI for years of 1986–2013 calculated using the NCEP-2 data (NCEP2-PNAI), with the PNA+ and PNA– months during 1999–2013 indicated. (b) PNAI for years of 1986–2013 calculated using the NCEP-2 data, with the PNA+ and PNA– months during 2000–2013 indicated. (c) PNAI for years of 1986–2006 calculated using the GEOS-4 data (GEOS4-PNAI), with the PNA+ and PNA– months over 1986–2006 indicated. Red circles are PNA+ months and blue circles PNA– months.

Fig. 3. The absolute ($\mu g\ m^{-3}$, left column) and relative differences (%, right column) in observed monthly mean aerosol concentrations between PNA+ and PNA– months (PNA+ minus PNA–). The measurements of $PM_{2.5}$ were carried out over 1999–2013, in which there were 18 PNA+ months and 18 PNA– months as shown in Fig. 2a. The measurements of speciated aerosols were taken during 2000–2013, in which there were 17 PNA+ and 17 PNA– months (Fig. 2b). The sites with black dots were the differences that passed the two-tail t-test with 90% confidence level.

Fig. 4. (a) Simulated surface-layer concentrations ($\mu g\ m^{-3}$) of $PM_{2.5}$ (the sum of SO_4^{2-}, NO_3^-, NH_4^+, BC, and OC) and each aerosol species averaged over NDJFM of 1999–2006. (b) Scatter plots of the simulated concentrations ($\mu g\ m^{-3}$, vertical axis) versus the EPA-AQS observations ($\mu g\ m^{-3}$, horizontal axis). Also shown are the y=x line (black dash line), linear fit for whole U.S. (black line), linear fit for western U.S. (blue line), and linear fit for eastern U.S. (red line). The blue and red dots represent sites in the western and eastern U.S., respectively. (c) Comparisons of the deviation from the mean (DM) of observed concentration (black line) with that of simulated concentration (red line) in each winter month for each aerosol species, left axis. Also shown in the panel for OC (BC) the monthly variation in DM of biomass burning emission of OC (BC), blue line, right axis.

Fig. 5. (a) Simulated concentrations ($\mu g\ m^{-3}$) of $PM_{2.5}$ and each aerosols species averaged over the PNA– months of 1986–2006. (b) The absolute differences ($\mu g\ m^{-3}$) in simulated aerosol concentrations between PNA+ and PNA– months (PNA+ minus PNA–). (c) The relative differences (%) in simulated aerosol concentrations between PNA+ and PNA– months. The white spaces in (C) indicate the areas that did not pass the two-tail student-t test with 90% significance level. The seasonal cycles of simulated aerosol concentrations were removed.

Fig. 6. (a) Horizontal winds at 700 hPa averaged over the winter months of NDJFM of 1986–2006, and (b) the corresponding differences between the PNA+ and PNA– months. Datasets are from the assimilated GEOS-4 meteorological fields. Also shown in (b) is the domain of (75–120°W, 28–49°N) for which transboundary mass fluxes of $PM_{2.5}$ are calculated.

Fig. 7. (a) The absolute and (b) relative differences in meteorological parameters between PNA+ and PNA– months. Datasets are from the assimilated GEOS-4 meteorological fields. The white spaces in indicate the areas that did not pass the two-tail student-t test with 90% significance level. The seasonal cycles of meteorological variables were removed, similar to the treatment for observations in Fig. 3.

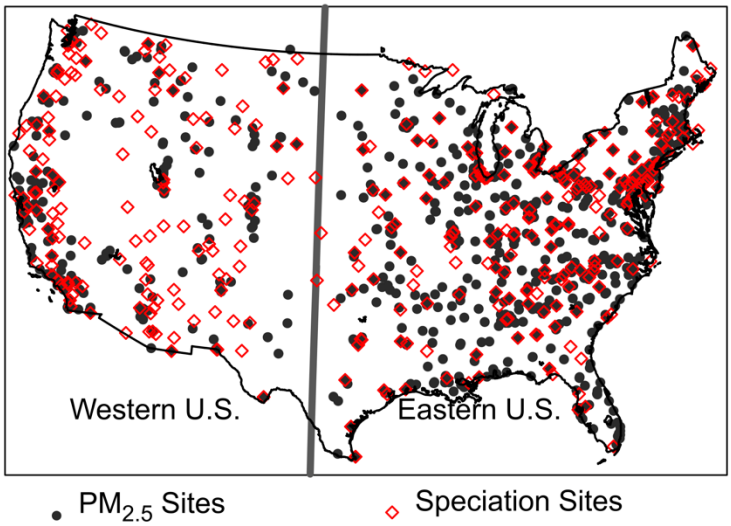

Fig. 1. The locations of EPA-AQS sites with measurements that meet the criteria described in Sect. 2.1 in the text. $PM_{2.5}$ measurements are available for years of 1999–2013 (sites are marked by black dots) and speciated aerosol (SO_4^{2-}, NO_3^-, NH_4^+, BC, and OC) concentrations are available over years of 2000–2013 (sites are marked by red diamonds). The grey solid line defines the western United States (west of 100°W) and eastern United States (east of 100°W).

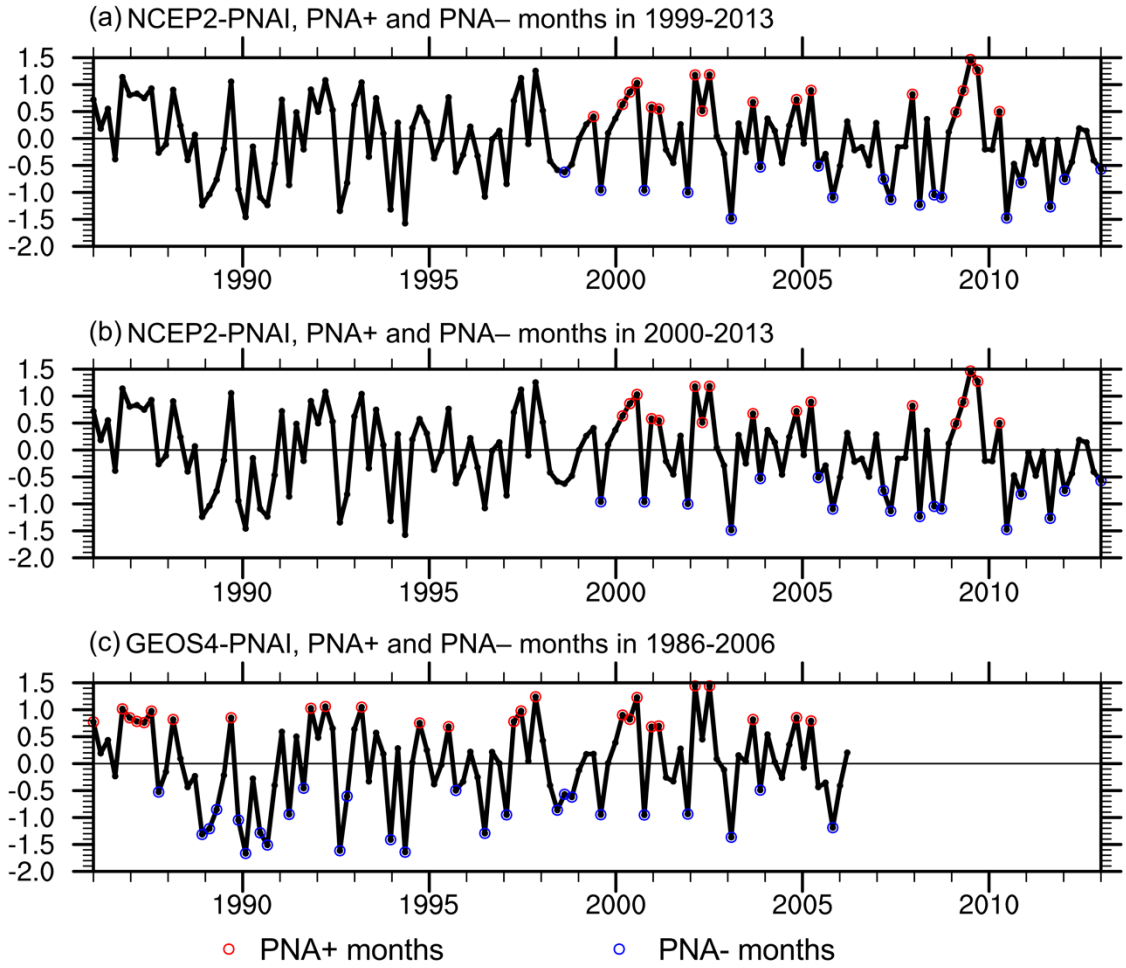

Fig. 2. (a) PNAI for years of 1986–2013 calculated using the NCEP-2 data (NCEP2-PNAI), with the PNA+ and PNA– months during 1999–2013 indicated. (b) PNAI for years of 1986–2013 calculated using the NCEP-2 data, with the PNA+ and PNA– months during 2000–2013 indicated. (c) PNAI for years of 1986–2006 calculated using the GEOS-4 data (GEOS4-PNAI), with the PNA+ and PNA– months over 1986–2006 indicated. Red circles are PNA+ months and blue circles PNA– months.

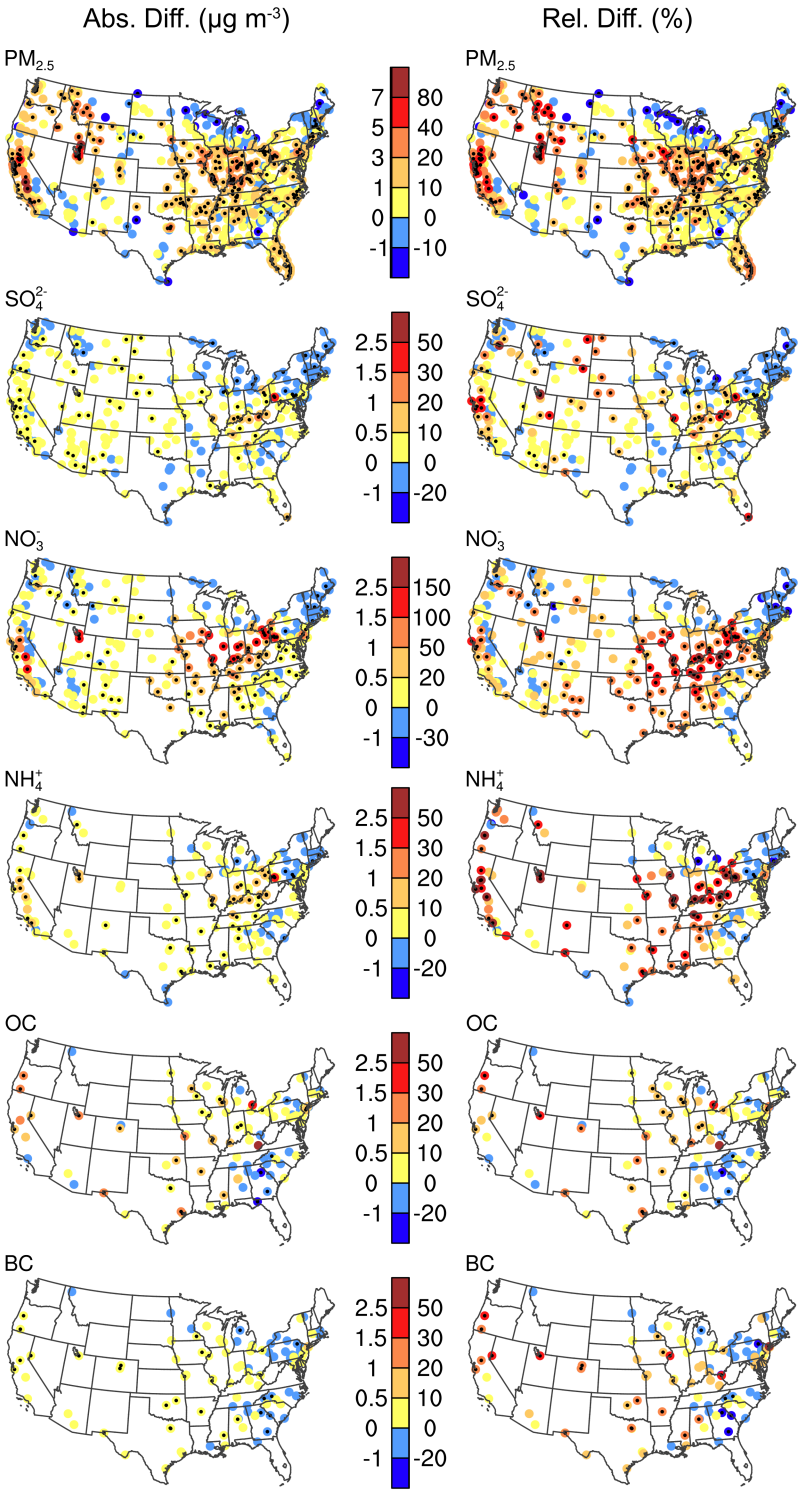

Fig. 3. The absolute (μg m^{-3}, left column) and relative differences (%, right column) in observed monthly mean aerosol concentrations between PNA+ and PNA– months (PNA+ minus PNA–). The measurements of $PM_{2.5}$ were carried out over 1999–2013, in which there were 18 PNA+ months and 18 PNA– months as shown in Fig. 2a. The measurements of speciated aerosols were taken during 2000–2013, in which there were 17 PNA+ and 17 PNA– months (Fig. 2b). The sites with black dots were the differences that passed the two-tail t-test with 90% confidence level.

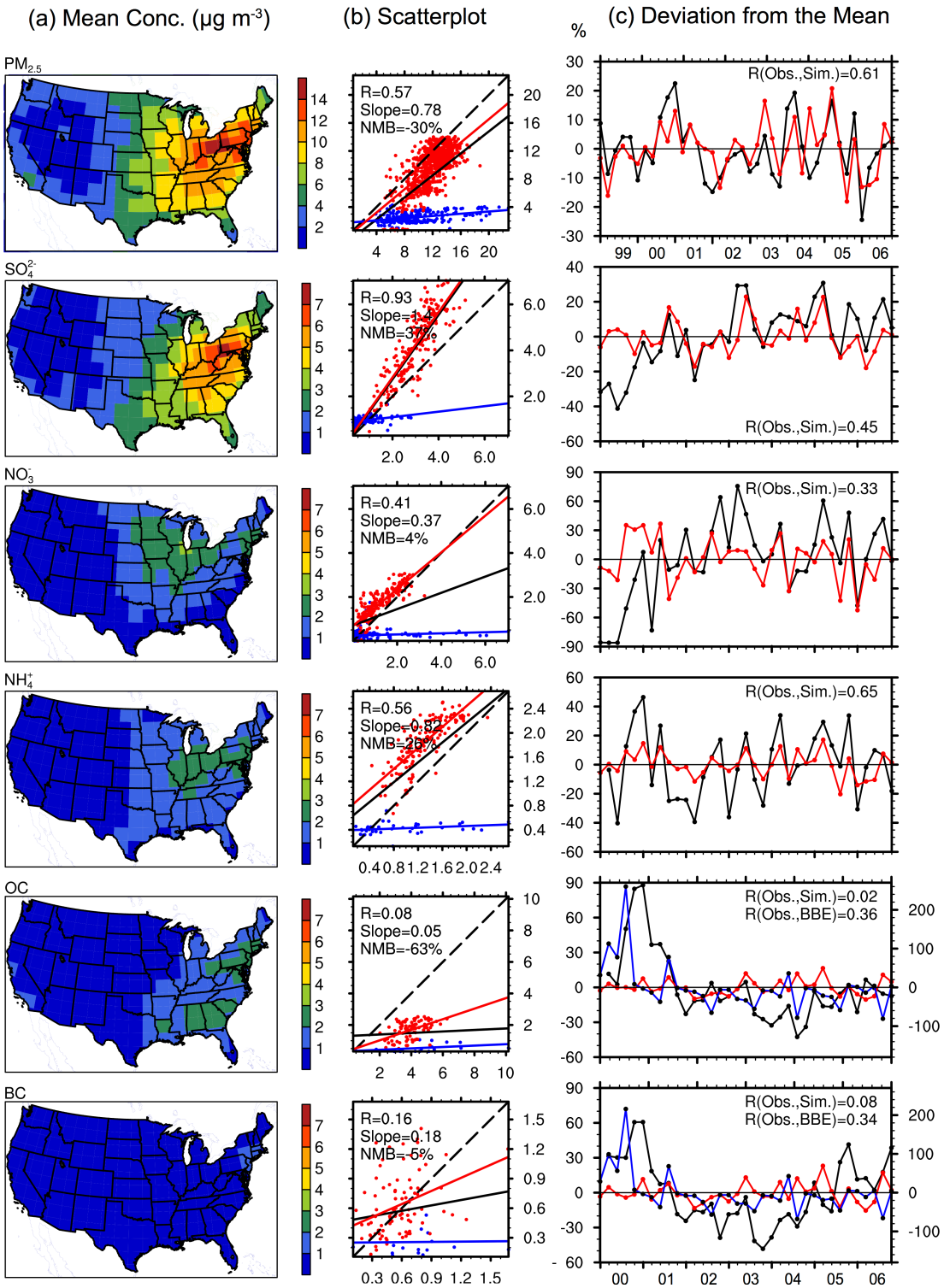

Fig. 4. (a) Simulated surface-layer concentrations (μg m^{-3}) of $PM_{2.5}$ (the sum of SO_4^{2-}, NO_3^-, NH_4^+, BC, and OC) and each aerosol species averaged over NDJFM of 1999–2006. (b) Scatter plots of the simulated concentrations (μg m^{-3}, vertical axis) versus the EPA-AQS observations (μg m^{-3}, horizontal axis). Also shown are the y=x line (black dash line), linear fit for whole U.S. (black line), linear fit for western U.S. (blue line), and linear fit for eastern U.S. (red line). The blue and red dots represent sites in the western and eastern U.S., respectively. (c) Comparisons of the deviation from the mean (DM) of observed concentration (black line) with that of simulated concentration (red line) in each winter month for each aerosol species, left axis. Also shown in the

1153 panel for OC (BC) the monthly variation in DM of biomass burning emission of OC
1154 (BC), blue line, right axis.

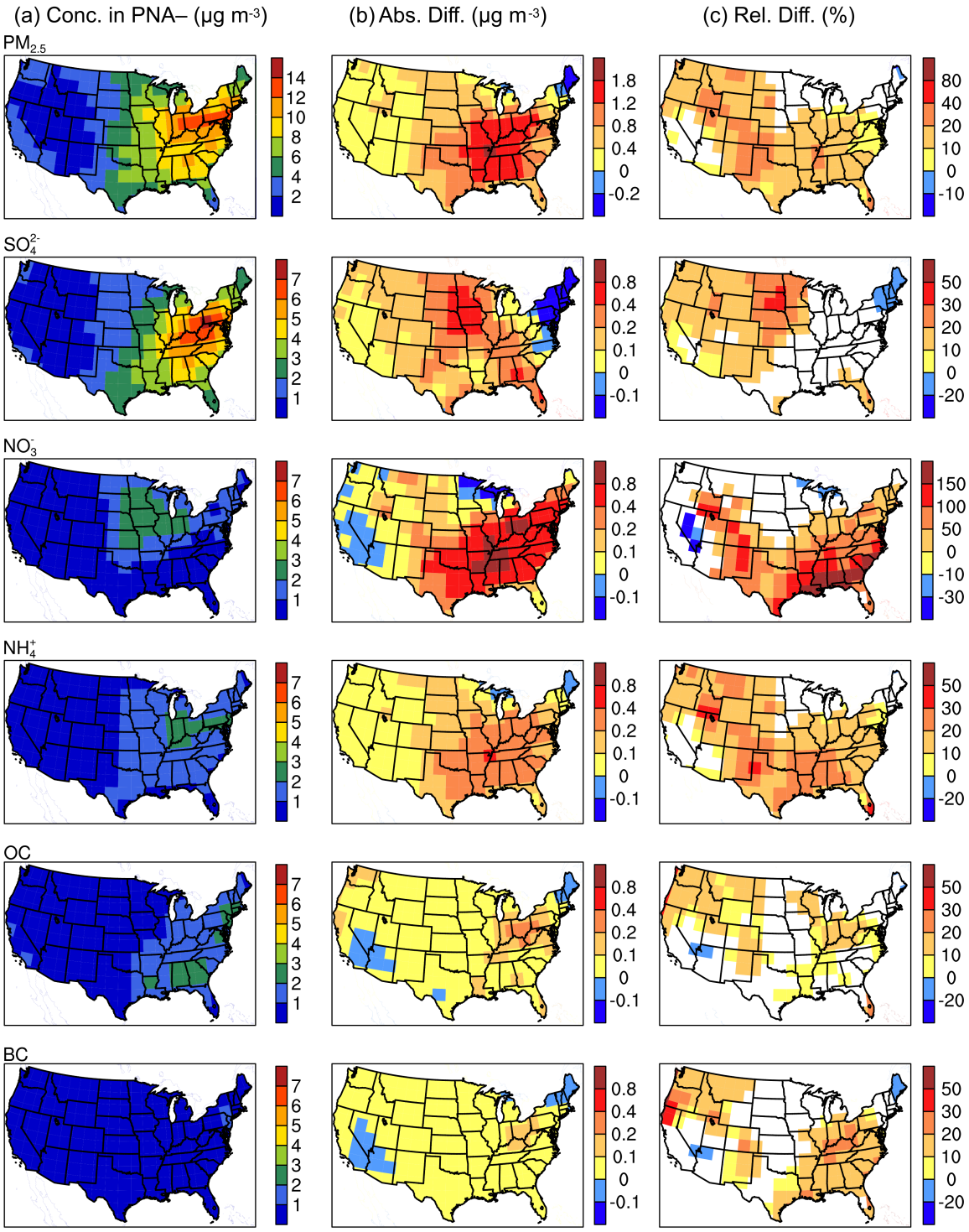

Fig. 5. (a) Simulated concentrations (μg m^{-3}) of $PM_{2.5}$ and each aerosols species averaged over the PNA– months of 1986–2006. (b) The absolute differences (μg m^{-3}) in simulated aerosol concentrations between PNA+ and PNA– months (PNA+ minus PNA–). (c) The relative differences (%) in simulated aerosol concentrations between PNA+ and PNA– months. The white spaces in (C) indicate the areas that did not pass the two-tail student-t test with 90% significance level. The seasonal cycles of simulated aerosol concentrations were removed, similar to the treatment for observations in Fig. 3.

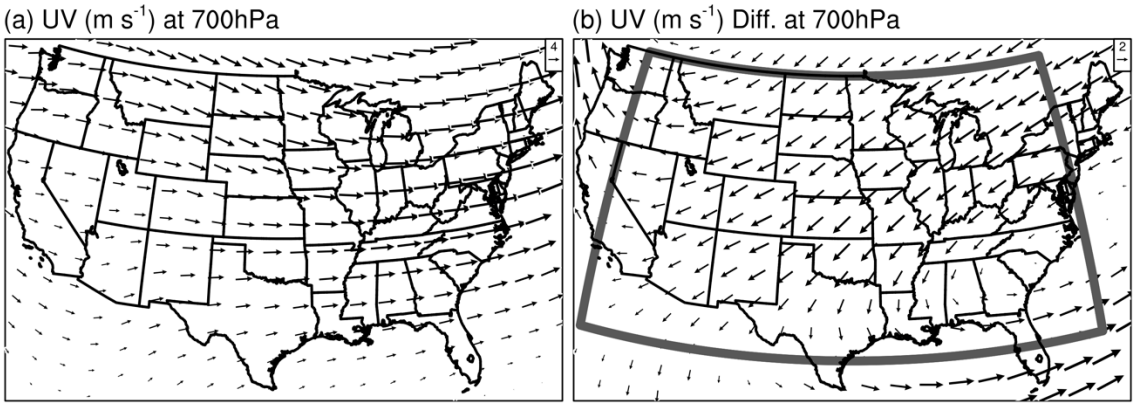

Fig. 6. (a) Horizontal winds at 700 hPa averaged over the winter months of NDJFM of 1986–2006, and (b) the corresponding differences between the PNA+ and PNA– months. Datasets are from the assimilated GEOS-4 meteorological fields. Also shown in (b) is the domain of (75–120°W, 28–49°N) for which transboundary mass fluxes of $PM_{2.5}$ are calculated.

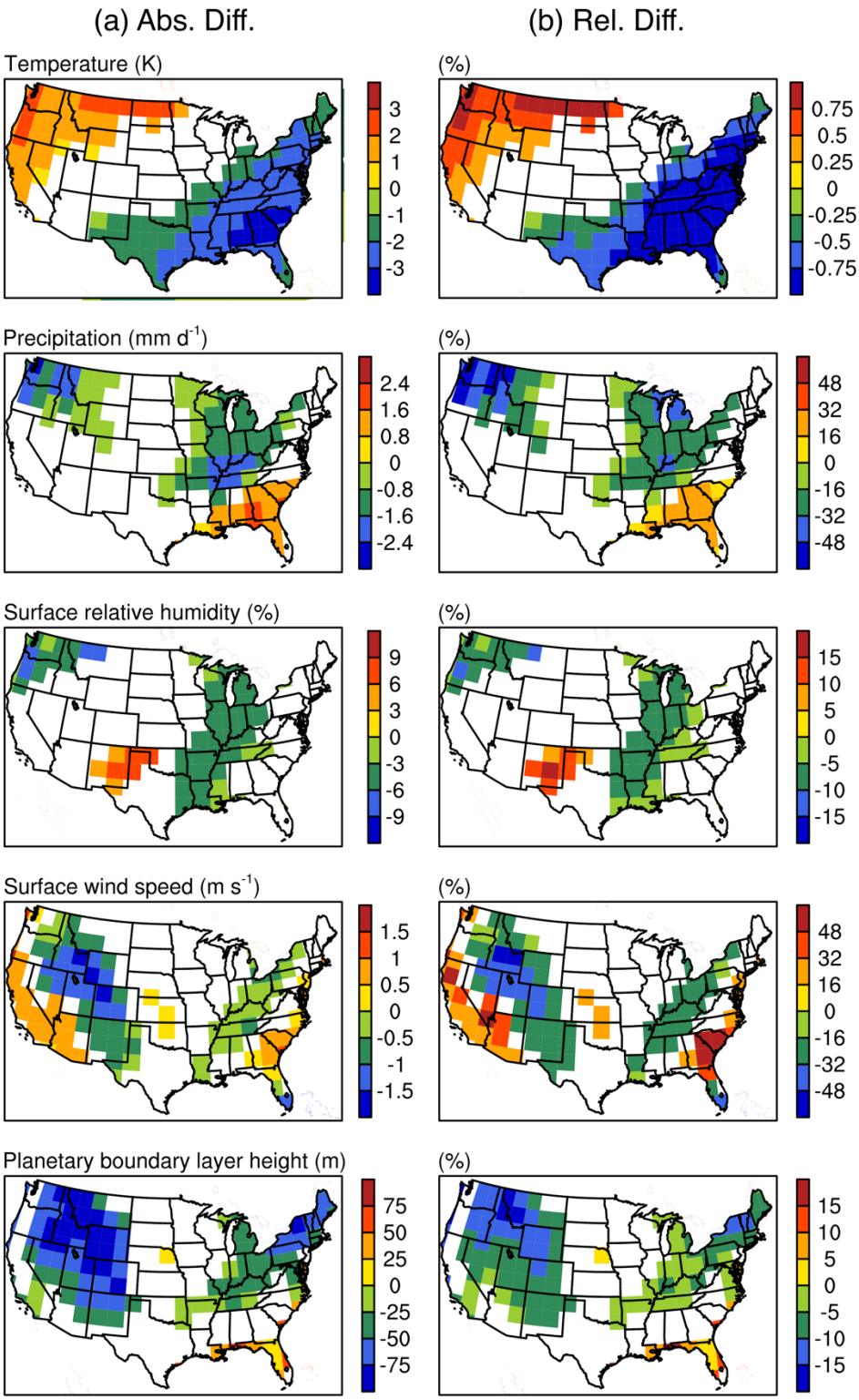

Fig. 7. (a) The absolute and (b) relative differences in meteorological parameters between PNA+ and PNA− months. Datasets are from the assimilated GEOS-4 meteorological fields. The white spaces in indicate the areas that did not pass the two-tail student-t test with 90% significance level. The seasonal cycles of meteorological variables were removed, similar to the treatment for observations in Fig. 3.